Computer model of metallic spin-glasses

L. R. Walker and R. E. Walstedt
Bell Laboratories, Murray Hill, New Jersey 07974
(Received 21 April 1980)

The low-temperature properties of dilute Ruderman-Kittel-Kasuya-Yosida (RKKY)-coupled spin systems have been investigated by computer simulation. Our results are based upon classical "ground states" for finite systems of spins distributed randomly in a cubic volume of fcc lattice, generated by an algorithm which lowers the system energy at each step. The (Heisenberg) RKKY exchange interaction is taken to be of the form appropriate to local moments in noble-metal hosts. In studying the number of such states which occur for a single system of 172 spins, we found only seven independent equilibrium configurations (EC's) among 70 which were generated from different random starting orientations. EC's are found to possess short-range angular correlation, such that a suitably defined correlation volume contains an average of $\sim$ two neighbor spins. The latter result is found to be independent of concentration, as expected for power-law range functions. The distribution $P_0(H)$ of exchange fields for EC's is compared with an analytic expression derived for randomly oriented spins in the dilute limit. The effect of ordering is to broaden the distribution by $\sim 50\%$ and to diminish the number of spins with very small fields. Quantum equations of motion for small oscillations about equilibrium are derived in a spin-wave approximation and are shown to be equivalent to their classical counterpart. Other features of the spin-wave picture are discussed. Low-lying modes related to rotational symmetry are discussed in detail in the Appendix. Calculated spectra are exhibited for systems of 96 and 172 spins and are found to scale correctly with concentration. Both local and dipolar anisotropy are found to introduce a zero-frequency gap in the excitation spectrum; the classical dipolar term is, however, too small to give an appreciable effect. A similar zero-frequency gap results from the application of a uniform field. Treating the excitations as bosons leads to a successful interpretation of specific-heat data for *Cu*Mn. For the case of *Au*Fe general agreement is also found, but with a discrepancy in form attributable to the Kondo effect. Damping of the RKKY interaction is found to cause a simple scaling of the excitation spectrum to lower frequencies. These results are used to interpret the concentration variation of the specific heat and the spin-glass ordering temperature for *Cu*Mn. We also employ EC's of 96 and 188 spins to calculate the zero-temperature reversible susceptibility, yielding good agreement with *Cu*Mn data (with $S=\frac{5}{2}$) and *Au*Fe data (with $S=\frac{3}{2}$).

I. INTRODUCTION

Despite the extensive efforts which have been devoted in recent years to the analysis of the spin-glass state it is fair to say that many important questions remain unanswered. The pioneering treatment by Edwards and Anderson[1] (EA) of a model with random-exchange interactions introduced some basic ideas about the possible nature of the spin-glass state, a plausible order parameter and a demonstration that the model would show, at least in mean-field theory, a phase transition. The cusp in the magnetic susceptibility observed by Canella and Mydosh[2] was also predicted to occur at the transition; a similar peak given for the specific heat is not observed experimentally.

Extensive Monte Carlo calculations by Binder[3] and Ching and Huber[3] on both Ising and Heisenberg systems show that the peak in the susceptibility may be reproduced. Binder also pointed out the relevance of a different order parameter based upon the zero-temperature configuration of the spins and studied its temperature dependence.[4] This work and some, but not all, experiments seem to leave open, however, the question of whether there is a genuine phase transition or, simply, a "blocking" effect indicative of extremely long relaxation times. A number of authors[5] have attempted to take into account, in simulations or in theory, the effect of clusters, defined rather loosely as groups of spins with strong correlations. There is some evidence that an explanation for the smoothness of the specific heat may be indicated in this work. There has been in addition, a great deal of effort expended upon highly idealized Ising models, which, significant in itself, does not immediately clarify the behavior of laboratory systems.

In the present paper we have attempted to explain some of the low-temperature behavior of spin-glasses

with Ruderman-Kittel-Kasuya-Yosida (RKKY) interactions making extensive use of computer simulation. These systems are reasonably well characterized and a good deal of experimental data is on hand. There is probably fairly general agreement that a disordered system of spins will, in the absence of excessive quantum fluctuations, possess a number of low-lying configurations nearly degenerate in energy. Because of the presence of energy barriers between these states one may expect them to exhibit some degree of permanence at sufficiently low temperatures. If the time spent by the system in any one of these configurations is long enough, it is reasonable to suppose that it will have a set of low-lying excitations analogous to those of an ordered spin system in its ground state. Since the system (and the configuration) have no translational invariance these excitations have no simple labeling by wave number; they belong exclusively to their parent configurations. In other respects they resemble magnons.[6] As the solution of a linearized set of equations of motion each mode is capable of independent and mutliple excitation; for thermodynamic purposes they may be treated as bosons. While these facts are formally clear their relevance to the properties of a real system depends upon a number of factors. It is clearly essential that the original ground-state configuration shall not be disrupted by zero-point effects or by migration over an energy barrier to another possible configuration. To be confident about the calculation of thermodynamic quantities one would need to know the extent to which the excitations interact, that is "How anharmonic is the system?"

In the present paper an attempt has been made to investigate some of these questions by numerical simulation of a real spin-glass system and, assuming the simple picture of noninteracting boson excitations, to evaluate some experimentally measured quantities. Initially we investigate configurations of a classical spin system which minimize the total energy.[7] Such configurations, analogous to the Néel state of an ordered antiferromagnet, provide a starting point for the discussion of excitations. The equations to be solved for the frequencies are the same in quantum and classical treatments. The excitations are then treated as bosons for thermodynamic purposes at sufficiently low temperatures. Since our initial report of this work[8] other studies along these same lines have been published.[9]

The question of the existence, number, and nature of classical minimum-energy states is obviously of considerable importance. Only if it is found that these states are nearly degenerate in energy and possess similar statistical distribution of properties is it reasonable to proceed with the second part of the program. These matters are therefore discussed in considerable detail in the first part of the paper.

In both the theoretical and experimental literature the term "spin-glass" has come to be applied in a very loose fashion to almost any disordered magnetic system exhibiting a susceptibility peak of acceptable acuteness. The term was originally applied to dilute, RKKY-coupled systems[10] of spins such as *Cu*Mn and *Au*Fe. We confine our attention here to systems of this type for a number of reasons. There is a considerable body of experimental data on magnetic susceptibility, remanence, magnetic time effects, specific heat, electrical conductivity, and magnetic resonance which covers a wide range of impurity concentrations. The interaction between the spins is well characterized and, in some cases, known in magnitude; in low concentrations, its variation with distance is such as to predict certain scaling rules with concentration and these are substantially verified. One finds therefore a favorable opportunity to compare calculated and experimental results.

The scaling laws for RKKY (or any r^{-3}) interaction potential require further comment. Attributed originally to Blandin[11] these are expected to apply strictly in the limit of considerable dilution ($c \ll 1.0$ at.%).[12] In that limit not only is the deviation from r^{-3} behavior at short range relatively unimportant, but also the cosine factor can be considered as an essentially random modulation not affecting the basic r^{-3} character of the coupling. It follows that the energies of the system increase linearly with concentration c, and for example, the reduced specific heat C_M/c and magnetization M/c are then functions of reduced field (H/c) and temperature (T/c) variables.[11] Other properties of RKKY spin-glasses are also expected to scale with c, as will be discussed in the body of this paper. Experimentally, spin-glass ordering temperatures for *Au*Fe have been found[13] to scale with c for c values between a lower limit determined by the Kondo effect and an upper limit $c \sim 1.0$ at.% which, we suggest, marks the onset of self-damping of the RKKY coupling by the Fe impurities themselves.[12] Curiously, the remanent magnetization also obeys scaling.[11]

While existing treatments of RKKY-coupled spin systems will be considered at appropriate points in the body of the paper, we offer one general comment at the outset. The RKKY interaction[10] is clearly understood to be of isotropic (Heisenberg) form. Nonetheless, many authors[14–18] have considered simplified treatments of RKKY-coupled systems in terms of the Ising approximation. This may give an adequate account of properties in the vicinity of the spin-glass temperature T_g and above; however, it is unlikely to yield valid results at low temperatures $0 < T < T_g$. In the latter case the properties of any isotropically coupled spin system are dominated by magnonlike excitations, and spin-glasses are presumably no exception.[8] Such excitations are only possible with transverse as well as z-axis coupling, making the Ising picture clearly inappropriate. In addition,

we find dramatic differences (Sec. II B) between the energies and distribution of Ising-like and isotropic ground states, further emphasizing the inadequacy of the Ising approximation.

The paper is organized in the following way. In Sec. II we discuss the computer generation of classical minimum-energy states and their properties. In Sec. III we examine the quantum-mechanical calculation of the excited states near to the energy minima, show its relation to the associated classical problem, and carry out in Sec. IV the calculation of excitation frequencies and eigenfunctions for a number of cases. The density of states of these modes and their spatial dependence are considered, as well as the effect of introducing self-damping of the RKKY interaction, dipolar and local anisotropy, and applied magnetic fields. The low-temperature specific heat and susceptibility are evaluated. Section V summarizes our results.

II. CLASSICAL MINIMUM-ENERGY STATES AND THEIR PROPERTIES

A. Formulation and methodology

It was pointed out in the Introduction that to make an analysis of low-energy excitations in the spin-glass one wants to start from configurations of the spins which are local energy minima. We start by considering this problem for a general Heisenberg system; extension to arbitrary two-spin interactions is straightforward, merely requiring more subscripts.

The classical Heisenberg spin system is to be represented by a collection of vectors $\vec{n}_i$, each of unit length, assigned to a set $\vec{r}_i$, of randomly selected sites of a regular lattice. The fraction of available sites occupied is c. The energy E is taken to be of the form

$$E = -\frac{1}{2}\sum_{i\neq j}\hat{J}(|\vec{r}_i-\vec{r}_j|)\vec{n}_i\cdot\vec{n}_j = -\frac{1}{2}\sum_{i\neq j}\hat{J}_{ij}\vec{n}_i\cdot\vec{n}_j \quad . \tag{2.1}$$

The specific choices of the interaction,[19] $\hat{J}(|\vec{r}|)$, and of the crystal lattice to be used in the simulation will be discussed below.

One is interested first in locating configurations, $\{\vec{n}_i\}$, for which the energy, $E\{\vec{n}_i\}$, has a local minimum. When these are found a number of questions may be asked. Some are as follows: In a system of a given size, how many such minima are found? Do the energies of such minima lie in a narrow range or not? Are the characteristics of these configurations, such as the distribution of field strengths, the range of correlation, and their excitation spectra, identical within statistical fluctuation? If the answers to the last two questions are affirmative, it will be reasonable to argue that the system has a number of essentially degenerate ground-state configurations.

If E is varied, subject to the constraints $\vec{n}_i\cdot\vec{n}_i=1$, the variational equations for stationary E are

$$\sum_j \hat{J}_{ij}\vec{n}_j = \hat{\lambda}_i\vec{n}_i \quad , \quad i=1,\ldots,N \quad , \tag{2.2}$$

where the $\hat{\lambda}_i$ are Lagrange multipliers. These equations have an obvious physical significance. $\sum_j \hat{J}_{ij}\vec{n}_j = \vec{h}_i$ is the exchange field which acts on spin i and Eq. (2.2) says that each $\vec{h}_i$ is parallel or antiparallel to $\vec{n}_i$ when E is stationary. A necessary, but in no way sufficient, condition for a configuration $\{\vec{n}_i^0\}$ satisfying Eq. (2.2) to be a local-energy minimum is that all associated $\hat{\lambda}_i$ be positive since this guarantees that changes in the orientation of any single spin will increase the energy. Similarly it can be shown that for stability against changes in the orientation of any pair of spins one must have $\hat{\lambda}_i\hat{\lambda}_j > (\hat{J}_{ij}\vec{n}_i^0\cdot\vec{n}_j^0)^2$ and so forth for larger groups. The full conditions for a configuration $\{\vec{n}_i^0\}$ to be a minimun can only be found by examining the change in energy E_2, to second order in the first-order displacements $\vec{m}_i$, when $\vec{n}_i^0$ is replaced by

$$\vec{n}_i^0+\vec{m}_i-\tfrac{1}{2}\vec{m}_i\cdot\vec{m}_i\vec{n}_i^0+\cdots \quad ,$$

where $\vec{n}_i^0\cdot\vec{m}_i=0$ and $|\vec{m}_i\cdot\vec{m}_i| \ll 1$. E_2 is given by

$$E_2 = \tfrac{1}{2}\sum_i \hat{\lambda}_i\vec{m}_i\cdot\vec{m}_i - \tfrac{1}{2}\sum_{i\neq j}\hat{J}_{ij}\vec{m}_i\cdot\vec{m}_j \quad . \tag{2.3}$$

Introducing at each occupied site a triad of mutually orthogonal unit vectors, $\vec{a}_i$, $\vec{b}_i$, $\vec{n}_i^0$ we may write

$$\vec{m}_i = \alpha_i\vec{a}_i+\beta_i\vec{b}_i \quad , \tag{2.4}$$

and E_2 becomes

$$E_2 = \tfrac{1}{2}\sum_i \hat{\lambda}_i(\alpha_i^2+\beta_i^2) - \tfrac{1}{2}\sum_{i\neq j}\hat{J}_{ij}(\alpha_i\vec{a}_i+\beta_i\vec{b}_i)\cdot(\alpha_j\vec{a}_j+\beta_j\vec{b}_j) \quad , \tag{2.5}$$

which is a quadratic form in the $2N$ variables α_i, β_i. If $\{\vec{n}_i^0\}$ is a true local minimum this must be nonnegative definite. Since, in the present Heisenberg case, the energy is invariant with respect to rotations of all the spins, the associated matrix of E_2 will have three zero eigenvalues corresponding to three independent rotations. The remaining $2N-3$ eigenvalues must be positive. The analytic expression of conditions for this to be true are unfortunately far too complicated to be put to practical use. It is, however, feasible to use a direct diagonalization of the E_2 matrix associated with a given configuration of the $\{\vec{n}_i^0\}$ as a verification of its minimum character.

There are exceptional classes of solutions to Eq. (2.2). The first of these is that of Ising states, for which each spin lies parallel or antiparallel to an arbi-

trary direction, $\vec{n}_0$. We may write $\vec{n}_i = \sigma_i \vec{n}_0$, with $\sigma_i = \pm 1$, for such states and then

$$\hat{\lambda}_i = \sigma_i \sum_j \hat{J}_{ij} \sigma_j \quad . \tag{2.6}$$

There are clearly 2^N such states where N is the number of spins. Whether or not any one of them is a local minimum involves exactly the same considerations as before. The quadratic form E_2 is now somewhat simpler in form but its properties again depend upon the particular set of $\hat{J}$'s involved. It may be noted that the Ising solutions represent a solution to the original optimization problem subject to an additional constraint, $\vec{n}_i^{\,0} = \pm \vec{n}_0$. The other class of solutions will be planar ones corresponding to the constraint $\vec{n}_i^{\,0} \times \vec{n}_0 = 0$. Again the existence of stable minima of this class has to be investigated for each case.

The location of possible energy minima by any direct solution of Eq. (2.2) seems not to be feasible. The apparent linearity of the equations is unhelpful when the side conditions, $\vec{n}_i^{\,0} \cdot \vec{n}_i^{\,0} = 1$, are recalled. Similar considerations arise if one thinks of applying standard minimization procedures to the original quadratic energy form in $3N$ variables.

Our approach was therefore to generate solutions of Eq. (2.2) which minimize E [Eq. (2.1)] by means of an iterative computer algorithm. For this we chose simply to rotate the spins sequentially into coincidence with their instantaneous fields $\vec{h}_i$ a sequence of N such rotations constituting a single iteration. While it would be possible to move two or more spins in a single step, the added complexity of such schemes renders the possible advantages questionable. Since the instantaneous energy at any point in the equilibration process can be written

$$E = -\vec{n}_i \cdot \vec{h}_i - \tfrac{1}{2} \sum_{j \neq k} \hat{J}_{jk} \vec{n}_j \cdot \vec{n}_k \quad , \quad j,k \neq i \quad , \tag{2.7}$$

where the entire dependence on E on $\vec{n}_i$ is embodied in the first term, the change ΔE resulting from rotating $\vec{n}_i \rightarrow \vec{h}_i / |\vec{h}_i|$ is simply

$$\Delta E_i = -(1 - \cos\theta_i) |\vec{h}_i| \quad , \tag{2.8}$$

where θ_i is the initial angle between $\vec{n}_i$ and $\vec{h}_i$. Thus, one is guaranteed a reduction in the system energy at every step with this algorithm. Rigorous analysis of this procedure is difficult because it acts on one spin at a time. However, since points in the configuration phase space which are stationary in energy, but are not true local minima (saddle points), have neighborhoods at lower energy, it is almost certain that an algorithm having some random character such as is used here will avoid such points.

In the present calculations $\hat{J}_{ij}$ is taken to have the form of the long-range part of the RKKY interaction,[10] or for two sites $\vec{r}_i$ and $\vec{r}_j$

$$\hat{J}_{ij} = A \cos(2k_F r_{ij}) / r_{ij}^3 \quad , \tag{2.9}$$

with $r_{ij} = |\vec{r}_i - \vec{r}_j|$ and k_F the Fermi wave vector. J_{ij} is truncated such that each spin interacts with an average of ~ 50 neighbor spins. More distant couplings affect equilibrium energies by 0.2% or less. The lattice is taken to be fcc and the lattice constant a, and free-electron wave vector k_F, are chosen to be those of Cu metal, with the application to *Cu*Mn in mind. Appropriate values for A will be given in Sec. IV.[20]

Equilibrium configurations (EC's) have been generated with the above procedure for systems containing $N = 96$ and ~ 180 spins randomly distributed in a cubic section of fcc lattice at concentrations of $c = 0.3$ at.% and 0.9 at.%. Periodic boundary conditions were imposed in order to minimize edge effects. In each case the spins were given random starting orientations and the algorithm iterated until no further reduction in E (outside roundoff fluctuations resulting from the eight-digit computer accuracy) could be achieved. The number of iterations required to reach equilibrium tended to increase with N and varied in individual cases from several hundred to more than 2000. The validity of the foregoing criterion for equilibrium was confirmed by diagonalizing the quadratic form [Eq. (2.5)] for the energy for small displacements from equilibrium. The absence of negative eigenvalues confirms that an energy minimum had been reached.

The behavior of E during equilibration consists of a rapid initial drop followed by a very slow and gradual decrease near equilibrium. We see from Eq. (2.8) that the steps ΔE_i become quadratically small as $\theta_i \rightarrow 0$. Meanwhile, the vectors $\vec{n}_i$ were found to execute relatively smooth trajectories on the unit sphere at small deviations from equilibrium. This was taken advantage of in the equilibration procedure by projecting the $\vec{n}_i$'s ahead along their trajectories every five or so elementary steps. A factor 2-3 in iteration time was saved in this fashion. Interestingly, it was found that even after the deviations θ_i had been reduced to less than 1° the $\vec{n}_i$'s were found to be displaced significantly from their final equilibrium orientations. In a typical case, for example, spins which deviated initially by a mean angle $\langle \theta_i \rangle \sim 0.2°$ from their exhange fields were found to rotate further through an average angle of $\sim 20°$ before reaching final equilibrium, during which the energy diminished by only $\sim 0.1\%$. Thus it appears that these systems are magnetically very soft, a fact which is undoubtedly related to the low-energy excitation peak reported in Sec. III.

B. Independent equilibrium configurations

One of the interesting questions regarding the formation of EC's is that of how many independent EC's can be found for a given spatial distribution of

N spins. An important related question is that of how independent EC's differ in detail. We have carried out an empirical examination of these questions using a single spatial distribution of $N=172$ spins. Since EC's have rotation and inversion symmetry, it was necessary to develop calculational machinery to distinguish genuinely independent EC's from those which differ only by a uniform rotation and/or inversion. We begin by describing the procedures used for this purpose.

To establish the "true" difference between a pair of EC's (denoted $\vec{n}_i$ and $\vec{n}_i'$, $i=1,\ldots,N$) we seek to minimize the two mean-square difference expressions

$$\Delta_{2\pm}=\frac{1}{N}\sum_i|\vec{n}_i'\pm R\,\vec{n}_i|^2 \ , \tag{2.10}$$

with respect to the rotation operator R, where the positive sign in Eq. (2.10) corresponds to having inverted one of the EC's. The minimum values of $\Delta_{2\pm}$ can also be expressed as

$$(\Delta_{2\pm})_{\min}\equiv 2(1-P_{\max}^{\pm}) \ , \tag{2.11}$$

where $P_{\max}^{\pm}$ is the maximum projection of the $\vec{n}_i'$ onto the $(\pm)R\,\vec{n}_i$, normalized so that $0\leq P_{\max}^{\pm}\leq 1$. The problem of determining R so as to minimize $\Delta_{\pm}$ is reduced in a straightforward manner to a 4×4 matrix eigenvalue problem. In the discussion below, comparisons of sets of EC's are presented by quoting values of $P_{\max}^{\pm}$.

With the methods of Sec. II A, 70 EC's were generated from independent randomly oriented starting configurations, out of which only seven unique members were found. Whether any of these would merge if the equilibration process were to continue with greater than eight-digit precision is a matter of conjecture. Thus there is a possibility that the number of independent EC's is smaller than 7. It is rather unlikely that it is larger, i.e., that there are additional independent EC's which did not occur in the random sample of 70 examined. In the simple case that all EC's have equal likelihood of being detected, the probability that there are Z independent EC's and only $Z-1$ occurred in a random sample of N_s starting configurations is

$$P_1(N_s)=Z(1-Z^{-1})^{N_s} \ . \tag{2.12}$$

For $Z=8$ and $N_s=70$, $P_1(N_s)=7.0\times 10^{-4}$. Further, the probability of two such EC's not occurring is

$$P_2(N_s)=\tfrac{1}{2}Z(Z-1)(1-2Z^{-1})^{N_s} \ , \tag{2.13}$$

which for $Z=9$ and $N_s=70$ is 8.2×10^{-7}, i.e., negligibly small. Of course, if there are one or more states with a statisitical weight of order N_s^{-1}, their probability of remaining undetected remains finite.

We have compared the members of our "complete" set of EC's in a variety of ways, including state energies, maximum mutual projection, and the number of spins on which the major differences between a pair of EC's resides. Considering these results in turn, we exhibit in Table I the energies of the EC's as well as the values of $P_{\max}$ for all 21 pairings. The energies are in reduced units.[20] The energies are seen to be very narrowly grouped, with a standard deviation of only 0.02% of the mean value. Since the exchange is of order unity at near-neighbor distances, the differences among EC's must be confined to variations in rather remote exchange bonds. For any fixed spatial distribution of spins the same narrow spread in the equilibrium energies is to be expected, but there may be a substantial discrepancy between the energies of different distributions. This is a finite-size effect principally arising from the statistically fluctuating numbers of spins with very strong interactions.

We have also studied the energies of Ising EC's to compare with the isotropic case. Ising equilibriums were generated in two distinct ways. In the first, the spins were restricted to lie along a particular direction in space. Beginning with the spins randomly up or down, a simple equilibrium is achieved by iteratively reorienting them to point along their local field. In

TABLE I. Energies and mutual projections $P_{\max}^{\pm}$ for the seven unique EC's of 172 spins described in the text. The larger of $P_{\max}^{\pm}$ is listed, with the notation $(-)$ when $P_{\max}^{-}>P_{\max}^{+}$. The mean energy $\langle E\rangle=-17.510\,191$ with a standard deviation $\langle\Delta E\rangle_{\rm sd}=1.8\times 10^{-4}\langle E\rangle$.

EC No.	1	2	3	4	5	6	7
	$E=-17.513\,388$	$-17.510\,368$	$-17.513\,006$	$-17.513\,483$	$-17.507\,343$	$-17.507\,633$	$-17.506\,113$
2	$P_{\max}=0.783$						
3	0.961(−)	0.811(−)					
4	0.749	0.826(−)	0.744(−)				
5	0.691	0.820(−)	0.709(−)	0.892			
6	0.925(−)	0.693(−)	0.906	0.747(−)	0.647(−)		
7	0.770(−)	0.877(−)	0.713	0.798	0.903	0.674	

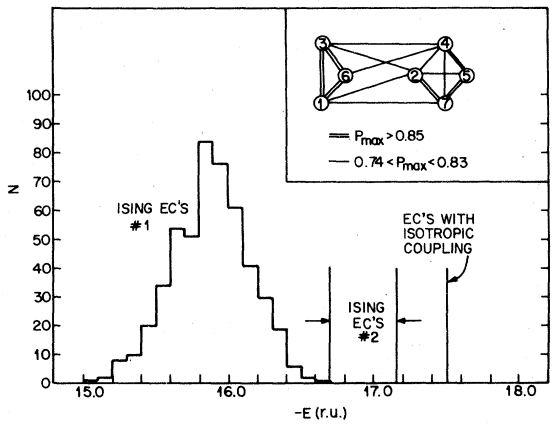

FIG. 1. Comparison of the energy distributions of two sets of Ising EC's (obtained as described in the text) with that of the seven unique isotropic EC's found for a specific spatial distribution of 172 spins at $c=0.9$ at.%. The inset shows a bond diagram for the seven EC's based on the P_{max} values in Table I.

Fig. 1 (Ising EC's No. 1) we display the energy distribution of several hundred Ising EC's generated in this fashion. The energies of these states are broadly distributed and well above those of the isotropic case. It is well known, however, that much lower Ising energies can be reached with special procedures. In case No. 2 we begin by first bringing an initially random set of spins into near-equilibrium with isotropic coupling. The transverse-coupling terms are then reduced linearly to zero over a space of 50 iterations. The resulting Ising EC's (No. 2 in Fig. 1) are below set No. 1 and more narrowly distributed in energy, but still well removed from the isotropic EC's. These results demonstrate that it is the isotropic character of the exchange which permits the EC's to be very nearly degenerate. We also conclude that it would be very unlikely to find an Ising state lower than the isotropic EC's.

The projections P_{max} are shown in Table I, with notation $(-)$ where an inversion was also required. P_{max} values are seen to range from 0.647 (columns 5 and 6) up to 0.961 (columns 1 and 3). For randomly oriented spins one finds $P_{max}\sim 0.1$, and thus, all seven EC's are seen to have a large region or regions of common orientation, with a number of pairs differing by ony a handful of deviated spins. On the basis of the P_{max} values of Table I, one can construct a "bond" diagram as in the inset to Fig. 1 showing that the EC's naturally divide into two groups on the basis of how large their mutual projections are, with weaker projections coupling to members of the opposite group. It is interesting to note that the groups in Fig. 1 are not ordered according to energies, so that proximity in orientation is not strongly correlated with closeness in energy.

One can also characterize pairs of EC's in terms of the numbers of spins over which their differences are distributed once they are rotated so as to maximize their mutual projection. For this purpose we introduce the mean fourth-power difference

$$\Delta_{4\pm}=\frac{1}{N}\sum_i |\vec{n}_i' \pm R\,\vec{n}_i|^4 \tag{2.14}$$

in the same notation as Eq. (2.10). We also define $\vec{n}_{mi}=\mp R\,\vec{n}_i$ to be rotated, and if necessary, inverted $\vec{n}_i$'s which minimize $\Delta_{2\pm}$. The corresponding values of $\Delta_{2\pm}$ and $\Delta_{4\pm}$ are denoted Δ_2 and Δ_4, respectively. Thus

$$\Delta_{2,4}\equiv\frac{1}{N}\sum_i |\vec{n}_i'-\vec{n}_{mi}|^{2,4}\ .$$

It is clear, then, that Δ_4 gives additional information as to how the differences $\vec{n}_i'-\vec{n}_{mi}$ are distributed over the N spins. To illustrate this we take a simple example where for N_D "deviated" spins

$$(\vec{n}_i'-\vec{n}_{mi})\cdot(\vec{n}_i'-\vec{n}_{mi})=d$$

and for the remaining $N-N_D$ spins, $\vec{n}_i'-\vec{n}_{mi}=0$. One then finds $\Delta_2=(N_D/N)d$ and $\Delta_4=(N_D/N)d^2$, so N_D can be expressed

$$N_D=N\Delta_2^2/\Delta_4\ . \tag{2.15}$$

In a general case we may take Eq. (2.15) as an approximate measure of the number of spins on which the difference between a pair of EC's is distributed. N_D values for the seven EC's discussed previously

TABLE II. N_D values computed from Eq. (2.15) for the seven independent EC's discussed in the text.

EC No.	1	2	3	4	5	6
2	48.3					
3	15.6	48.4				
4	46.7	79.0	50.4			
5	58.3	63.4	59.8	24.9		
6	21.0	61.0	26.8	49.5	65.4	
7	56.0	27.6	63.9	49.5	48.9	82.7

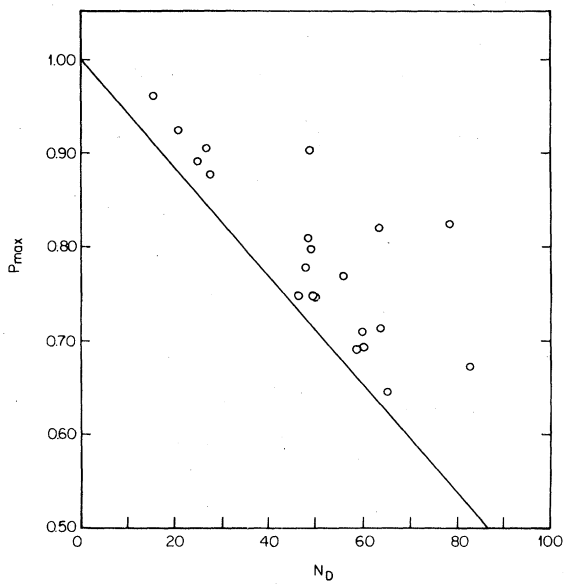

FIG. 2. Plot of P_{max} vs N_D for all possible pairings of the seven unique EC's as given in Tables I and II. The line drawn corresponds to N_D spins with zero mutual projection and $N - N_D$ spins with a projection of unity.

are given in Table II, where they are seen to vary from the minimum of 15.6 to a maximum of 82.7.

Comparison of P_{max} values in Table I with N_D values in Table II suggests that these quantities are strongly correlated. This effect is illustrated in the plot of P_{max} vs N_D in Fig. 2. The straight line in Fig. 2 corresponds to having the N_D "deviant" spin pairs at an average angle of 90° to one another (i.e., with zero mutual projection) with the other $N - N_D$ spins perfectly aligned. The actual behavior lies above this curve, so that the mean angle between the N_D spins is somewhat less than 90°. Interestingly, points in Fig. 2 corresponding to pairs of *random* spin distributions fall well below the curve at $P_{max} \sim 0.1$ and $N_D \sim 120$. Even the most disparate of the EC pairs does not approach these parameter values.

The data of Tables I and II show that the extent of differences between pairs of EC's of 172 spins can vary over wide limits. It is noteworthy that the *minimum* deviation between independent EC's is found to occupy nearly 16 spins. While it is possible that a smaller minimum number would occur for a different spatial distribution, it appears that the minimum cluster size which can achieve different states of ordering is many correlation volumes in size (see Sec. II C, where it is shown that a correlation volume contains ~2 spins).

C. Range of angular correlations

The equilibrium states we have found represent a cooperative effort of the interacting spin system to reduce its total energy. Clearly, because of the spatial disorder, the resultant states can show no obvious pattern of organization. Visual examination of the array of spin vectors in an equilibrium state has suggested evidence for various types of local structure in the pattern to various observers. To test for such properties is very time consuming. If the local structure exists it implies that the vector $\vec{n}_i$ is related on the average to another vector $\vec{n}_j$, in some way which depends upon the vector $\vec{r}_i - \vec{r}_j$, joining their sites. Only if some specific assumption is made about the form of this relation can it be tested, and there are far too many possible assumptions. We have, therefore, analyzed only the simplest parameter of this type, namely the angular correlation or average of $\vec{n}_i \cdot \vec{n}_j$ over all sites with a fixed separation, $|\vec{r}_i - \vec{r}_j|$.

The range of angular correlation may be roughly characterized by a correlation volume Ω_c within which spin alignment is substantial. We discuss different measures of Ω_c, beginning with a simple physical model to elucidate the factors which determine this fundamental quantity. One may estimate Ω_c by assuming that a spin $\vec{n}_0$ at the origin will be strongly correlated with spin $\vec{n}_i$ at $\vec{r}_i$ if the coupling $\hat{J}_{0i}$ is stronger than the net exchange field at $\vec{n}_0$ caused by more distant spins. Since $\hat{J}_{0i} \propto r_i^{-3}$, whereas the rms field from spins at $r_j > r_i$ varies approximately as $r_i^{-3/2}$, there will be a crossover point $r_i = r_c$ between these (suitably averaged) fields which we shall use to estimate the correlation volume. Denoting the rms field from sites at $r_j > r$ as $\hat{J}_{rms}(r)$, we have

$$\hat{J}_{rms}(r) = \left\langle \sum_{j(\mathrm{occ}),\, r_j > r} \vec{n}_j \hat{J}_{0j} \right\rangle_{rms} , \tag{2.16}$$

where for simplicity we average over RKKY phase and all possible neighbor configurations (occ = occupied). Using Eq. (2.9) for $\hat{J}_{ij}$ we find for the correlation volume

$$\Omega_c = \tfrac{4}{3}\pi r_c^3 = 2a^3/\pi^2 c \ . \tag{2.17}$$

Thus the mean number of neighbors in a correlation volume is $8/\pi^2$, independent of concentration. Interestingly, the latter property, which is implied by the form $\Omega_c \propto c^{-1}$, holds for any power-law variation of $\hat{J}_{ij}$ for which the system is stable. Thus, it is more general than the scaling laws described in Sec. I. One also notes that the correlations are strikingly weak, with each spin only being strongly aligned on the average with a single neighbor.

As noted above, the ground-state energy is a consequence and thus in some sense also a measure of angular correlation. For a large system we can rewrite Eq. (2.1) in terms of the average values $\langle \vec{n}_i \cdot \vec{n}_j \rangle_n$ of $\vec{n}_i \cdot \vec{n}_j$ over all nth neighbor pairs in the lattice

$$E = -\tfrac{1}{2} N c \sum_n Z_n \hat{J}_n \langle \vec{n}_i \cdot \vec{n}_j \rangle_n \ .$$

By introducing the correlation coefficient

$$C_n = \mathrm{sgn}(\hat{J}_n)\langle \vec{n}_i \cdot \vec{n}_j \rangle_n \tag{2.18}$$

for nth neighbors, the energy becomes

$$E = -\tfrac{1}{2} Nc \sum_n C_n Z_n |\hat{J}_n| \ , \tag{2.19}$$

where Z_n is the number of sites in the nth neighbor shell, $\hat{J}_n$ is the corresponding exchange constant, and c is the occupation probability per site. As defined in Eq. (2.18), one expects $C_n \geq 0$, but C_n will not necessarily be smoothly varying. Using Eq. (2.19) one may again make a rough estimate of the correlation volume, using in this instance energies of simulated EC's. For this purpose we take the simple form

$$C_n = \begin{cases} 1, & r_n < r_c \ , \\ 0, & r_n > r_c \ , \end{cases} \tag{2.20}$$

where r_n is the separation of nth neighbor pairs. With Eq. (2.20), the energy becomes simply

$$E = -\tfrac{1}{2} Nc \sum_{n=1}^{n_c} Z_n |\hat{J}_n| \ , \tag{2.21}$$

where n_c is the neighbor shell index corresponding to r_c [$r_c = a(\frac{1}{2} n_c)^{1/2}$ for the fcc lattice]. In Fig. 3 we plot Eq. (2.21) on scales of E vs $\log_{10}(n_c)$ for the case of ten independent spatial distributions of 188 spins each at a concentration of $c = 0.30\%$. Thus $N = 1880$ and the Z_n's are combined values for all ten distributions. Equation (2.21) diverges as $\log_{10}(n_c)$ in the continuum limit, a behavior which is shown as a straight line in Fig. 3. The combined energy of the ten EC's generated (one for each spatial distribution) is shown as a dashed line in the figure, giving a value of $n_c = 25$ for the neighbor shell enclosing the correlation volume as defined by Eq. (2.21). It follows that the correlation volume defined this way contains 2.2 neighbor spins, i.e., about twice the number obtained using Eq. (2.17).

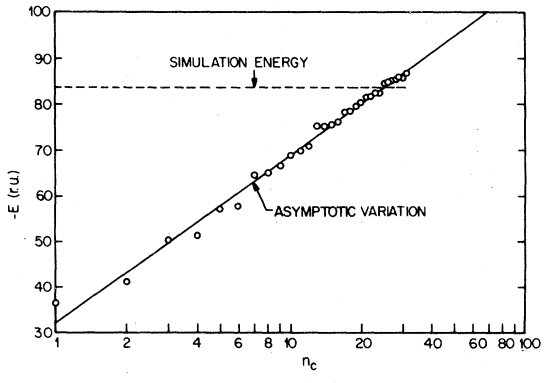

FIG. 3. Plot of $-E(n_c)$ from Eq. (2.21) in the text vs $\log_{10}(n_c)$ for $1 \leq n_c \leq 31$, using energies and z_n data from ten distributions of 188 spins each at $c = 0.3$ at.%. The straight line represents the asymptotic (continuum limit) variation $E = -2\sqrt{2}Nc \log_{10}(n_c) + C_0$, where C_0 is adjusted to produce agreement at large n_c.

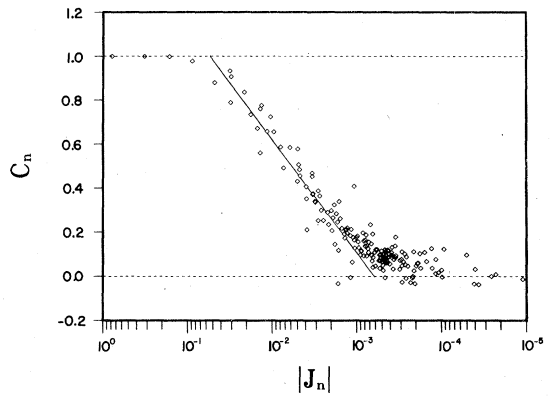

FIG. 4. Plot of C_n [Eq. (2.18)] vs $\log_{10} J_n$ for $1 \leq n \leq 90$ using average correlation data from ten spatially independent EC's of 188 spins each at $c = 0.3$ at.%. The straight line is for comparison purposes only.

Perhaps the most direct method of measuring angular correlation is to plot mean values of C_n [Eq. (2.18)] derived from the simulation mentioned above. It is not clear at the outset whether C_n is determined by the distance r_n or the coupling $\hat{J}_n$ of the nth neighbor shell. To investigate this point we plot the C_n data against the logarithm of $\hat{J}_n$ in Fig. 4 and that of r_n^{-3} (which mimics the variation of $\hat{J}_n$) in Fig. 5. Although there is scatter in both cases, it is clear that $\hat{J}_n$ is a stronger influence on C_n than r_n. While some of the scatter in Fig. 4 is statistical, it seems unlikely that C_n is *exclusively* a function of $\hat{J}_n$. Data from a much larger simulation volume are needed to examine this question further.

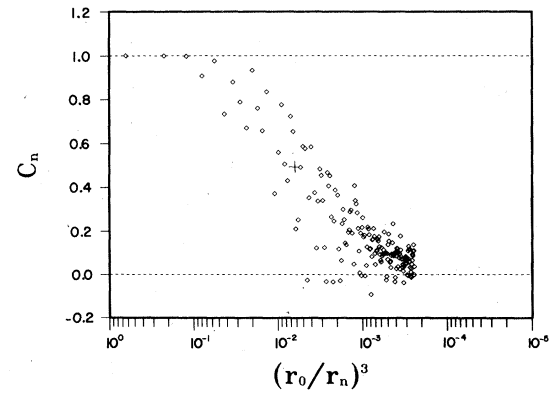

FIG. 5. Plot of C_n [Eq. (2.18)] vs $\log_{10}(r_0/r_n)^3$, where the abscissa is the logarithm of J_n with $\cos(2k_T r_n)$ replaced by its average magnitude. The cross is used to estimate the correlation volume.

The foregoing discussion demonstrates that the concept of a spherical correlation volume surrounding a given site is rough even on a large system average, since there will be weakly correlated spins within such a volume and strongly correlated ones outside. Nonetheless, we may estimate an approximate correlation volume with Fig. 5 by taking the radius where the middle of the C_n distribution drops to $C_n \sim 0.5$. This point is indicated by a cross. The resulting volume contains 1.8 neighbors, only slightly smaller than the number estimated from EC energies using Fig. 3.

We have also obtained correlation data for ten spatial distributions containing 177 spins each at $c = 0.9$ at.%. Corresponding values of C_n are plotted versus $\log_{10}|\hat{J}_n|$ in Fig. 6 as they are in Fig. 4. The correlation curve in Fig. 6 is moved to larger $|\hat{J}_n|$ values as expected for a higher concentration. If we consider the $|\hat{J}_n|$ scales in Figs. 4 and 6 to be approximate inverse volume scales, then by the scaling laws outlined in Sec. I, the correlation curves should (in the dilute limit approximation) be parallel and displaced from one another by a factor of 3 on the $\hat{J}_n$ axis. The straight lines drawn through the data in these figures are so constructed and illustrate that the scaling effect is well obeyed.

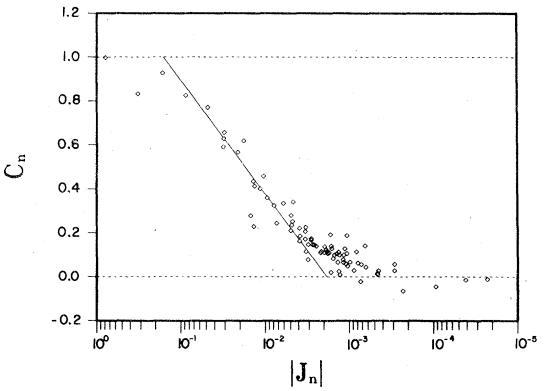

FIG. 6. Plot of C_n [Eq. (2.18)] vs $\log_{10}(J_n)$ for $1 \leq n \leq 180$ using average correlation data from ten spatially independent EC's of 177 spins each at $c = 0.9$ at.%. The straight line drawn is parallel to that in Fig. 4 and shifted to values of $|J_n|$ smaller by a factor of 3.

We also wish to point out that there is considerble information in the raw correlation data that is lost in the averages presented in Figs. 4–6. To illustrate this we present in Table III a two-dimensional histogram of regional occupation probabilities in the C vs $\log_{10}|\hat{J}|$ plane of Fig. 4, where the numbers in each $\hat{J}$

TABLE III. The data used to compute the average correlations in Fig. 4 are presented as regional occupation probabilities in the C vs $\log_{10}(J)$ plane. Correlation intervals are defined as shown on the left and the $\log_{10}(J)$ scale of Fig. 4 has been divided into ten intervals, where the first is $10^{-1/2} \leq J < 1$, etc. The probabilities of any column sum to unity, with the total number of neighbor pairs in each is shown in the bottom row.

		$l=1$	2	3	4	5	6	7	8	9	10
	1.0										
		1.000	1.000	0.925	0.793	0.472	0.255	0.159	0.140	0.126	0.118
	0.8										
		0	0	0.018	0.055	0.130	0.139	0.120	0.110	0.104	0.102
	0.6										
		0	0	0.014	0.033	0.074	0.099	0.108	0.097	0.092	0.106
	0.4										
C_l		0	0	0	0.014	0.059	0.089	0.098	0.096	0.095	0.087
	0.2										
		0	0	0	0.018	0.043	0.074	0.091	0.091	0.093	0.095
	0.0										
		0	0	0.014	0.010	0.039	0.073	0.086	0.088	0.083	0.081
	−0.2										
		0	0	0.005	0.012	0.041	0.056	0.095	0.091	0.086	0.080
	−0.4										
		0	0	0.005	0.012	0.029	0.060	0.089	0.092	0.100	0.098
	−0.6										
		0	0	0.009	0.014	0.043	0.068	0.085	0.092	0.098	0.098
	−0.8										
		0	0	0.009	0.039	0.073	0.086	0.092	0.103	0.122	0.135
	−1.0										
N_l		61	56	211	862	2038	7415	18702	10915	1772	1683

interval (column) are normalized to unity. It is interesting to note significant deviations from uniform (random) probability even for the column (No. 10) in the table representing weakest coupling. Further, there is also a significant excess probability for spin pairs aligned *opposite* to their exchange coupling (bottom row of Table III). This would appear to arise out of strongly correlated clusters (of 3 or more) when conflicting bonds are the inevitable result of "frustration" inherent in the bond topology of spin-glasses.

D. Internal field distributions

The distribution of internal-exchange fields played a major role in early models of spin-glass heat capacity, which is proportional to the density of nearly vanishing fields in single-particle theories.[14–16] It is of interest to examine these distributions both from that standpoint and as a foundation for the elementary excitation spectra derived in Sec. III. In order to study the effect of ordering on field distributions, we first consider the case of randomly oriented, static spins.

In contrast with the ordered case, the case of random spins can be treated in a straightforward manner in the dilute limit. The corresponding field distribution $P_r(H)$ was first derived by Rivier and Adkins[16] for the special case of an exchange coupling which varies randomly in sign. We present a derivation of a more general result using methods applied earlier to the problem of RKKY hyperfine broadening in random alloys.[12] This technique begins with the relation $P_r(\vec{H}) = \langle \delta(\vec{H} - \vec{H}_i) \rangle$, where $\vec{H}_i$ is the field at a typical occupied site and $\langle\ \rangle$ denotes an average over all sites and all possible orientations of the spins. Using an integral representation of the δ function one has

$$P_r(\vec{H}) = \frac{1}{(2\pi)^3} \int d\vec{k}\, e^{i\vec{k}\cdot\vec{H}} \langle e^{-i\vec{k}\cdot\vec{H}_i} \rangle \ . \qquad (2.22)$$

We represent $\vec{H}_i = \sum_j x_j \hat{J}_{ij} \vec{n}_j$, where $x_j = 1$ if site j is occupied, 0 otherwise. Then the average $\langle\ \rangle$ in Eq. (2.22) becomes

$$\pi_j \langle \exp(-x_j \hat{J}_{ij} \vec{n}_j \cdot \vec{k}) \rangle_j \cong \exp\left[-c \sum_j \left[1 - \frac{\sin(\hat{J}_{ij} k)}{\hat{J}_{ij} k} \right] \right] , \qquad (2.23)$$

where $\langle\ \rangle_j$ is the occupational and orientational average for site j and the equality holds in the limit of small $c = \langle x_j \rangle$. In this limit the lattice sum in Eq. (2.23) can be represented as an integral. Using the same low-concentration approximation as in earlier work,[12] the rhs of Eq. (2.23) is shown in a straightforward fashion to be asymptotically given by $\exp(-\eta k)$, with

$$\eta = 8\pi c A / 3a^3 \ , \qquad (2.24)$$

where $\hat{J}_{ij}$ was taken from Eq. (2.9). Substituting back into Eq. (2.22) one immediately obtains

$$P_r(\vec{H}) = (\eta/\pi^2)(\eta^2 + H^2)^{-2} \ .$$

Spherical symmetry leads further to $P_r(H) = 4\pi H^2 P_r(\vec{H})$ and thus

$$P_r(H) = (4\eta/\pi) H^2/(H^2 + \eta^2)^2 \ . \qquad (2.25)$$

Equation (2.25) has been derived by Held and Klein[21] as the "random molecular-field approximation" to the field distribution in a spin-glass. As we have shown, it corresponds to totally random spins. In Fig. 7, Eq. (2.25) is compared with a computer-generated histogram of fields corresponding to 25 independent sets of random orientations of 324 spins in a single spatial distribution at $c = 0.3$ at.%. The field scale is in reduced units (ru).[20] The only fitting procedure used in Fig. 7 was to equalize the areas under the curves. The simulated curve is seen to agree with Eq. (2.25) within statistical error except in the vicintity of $h \sim 0.05$ ru, where a weak satellite is found, attributable to the seventh neighbor shell. It is not surprising to find a visible satellite at concentrations as high as this.[12]

The field distribution $P_0(H)$ for ordered spins is illustrated in Fig. 8, where we show a composite histrogram of molecular fields for EC's from the 10 spa-

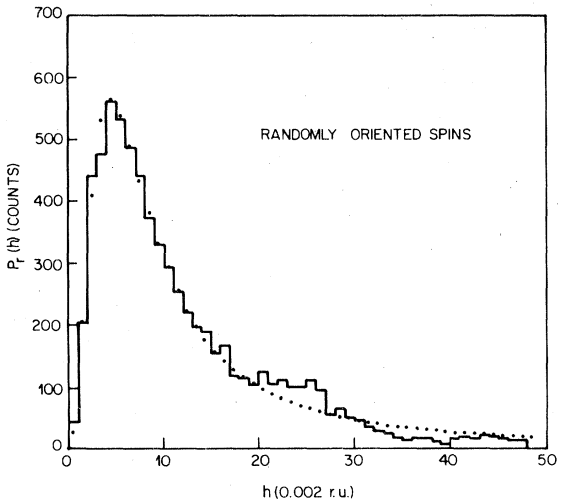

FIG. 7. Comparison of computer-generated histogram of exchange fields with Eq. (2.25) from the text (dots). Histrogram results are derived from 25 independent spatial distributions of 324 spins each at $c = 0.3$ at.%.

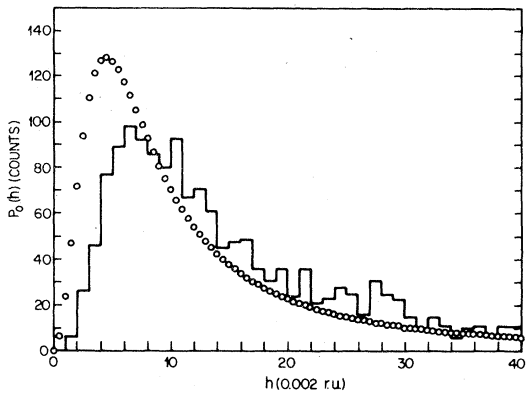

FIG. 8. Histogram distribution of exchange fields derived from EC's for ten independent spatial distributions of 188 spins at $c = 0.3$ at.%. The dots show the random-spin curve [Eq. (2.18)] normalized to the same area as $P_0(H)$.

tial distributions of 188 spins ($c = 0.3$ at.%) used earlier to generate the data for Figs. 4 and 5. We also plot for comparison the random spin curve Eq. (2.25) with its area normalized to the same value as the histrogram. The main effects of ordering are seen to be a shift in $P_0(H)$ to fields larger by a factor ~ 1.5 and a vanishing of spins with very small fields. As noted earlier[8] these effects can be understood in terms of the correlation phenomena discussed in Sec. II C. Using the correlation factor Eq. (2.18) the exchange field at site i can be seen to consist of two contributions, namely a correlated component

$$H_i^{\text{corr}} = \sum_{j(\text{occ})} |\hat{J}_{ij}| C(r_{ij}) \ , \tag{2.26}$$

where each neighbor is assumed to contribute an amount proportional to the correlation coefficient for that site, and an uncorrelated or random component which will only serve to broaden the distribution of H_i^{corr} values. Because the correlations are strong for $\hat{J}_{ij}$'s near the peak of $P_0(H)$ (see Fig. 4), the correlated components dominate $P_0(H)$ and the broadening effect of the random field contributions is relatively slight. With Eq. (2.26) we can understand the qualitative features of $P_0(H)$. The general increase in magnitudes comes from the fact that Eq. (2.26) sums absolute magnitudes of contributions which would otherwise combine randomly. The extent of this increase is limited to a factor of $\sim \sqrt{2}$ since there are, from Sec. II C, an average of only ~ 2 contributions from within the correlation volume. Furthermore by Eq. (2.26) it is relatively difficult to have nearly zero field at a site since this requires a large volume around that site to be unoccupied. Hence, very small fields are quite rare.

The appearance of a "hole" in the distribution $P_0(H)$ at zero field has been noted before.[8,22] It is contrary to suggestions that the ordered state would be Ising-like[15,16] and thus have a finite density of spins at $H = 0$ as assumed in the specific-heat model of Marshall.[14] Thus, we do not expect the single-particle theory of specific heat to be viable on the basis of the present results. Moreover, the vanishing of $P_0(H)$ as $H \to 0$ is thought to be true for Ising systems[23] as well as for isotropic exchange.

III. ELEMENTARY EXCITATIONS OF A SPIN-GLASS

The procedure of spin-wave theory as familiarly used for ordered spin systems is the following. A ground state is assumed which has each spin $\vec{S}_i$, of magnitude S, in a state such that $S_i^{z_i} = S$, where the local axis of quantization z_i, has some assigned direction in space. These directions are usually clearly indicated by symmetry. The spin operators are now expanded in boson operators, $c_i^\dagger$ and c_i, following the method of Holstein and Primakoff or its equivalent. In the Hamiltonian, terms up to second order in $c^\dagger, c$ are retained. A check on the fitness of the assumed ground state is the vanishing of all linear terms in c and $c^\dagger$. The procedure is essentially an expansion in powers of S^{-1}; it is justified, in part, when one calculates a new ground state and shows that it is not radically different from the original. Further justification requires that one show that higher-order terms in the Hamiltonian, leading to finite lifetime, scattering, and frequency renormalization effects, are not obtrusive in the physical context. There appears to be no reason why a formally similar program cannot be carried through for the spin-glass. However, any evaluation of the validity of the result as an approximation to the physical situation is obviously a very difficult problem in the absence of simplifying symmetries. Beyond an examination of the zero-point effects we shall not attempt to deal with these questions.

To avoid unnecessary complications we consider for the moment only isotropic exchange interactions. Thus the Hamiltonian is

$$H = -\tfrac{1}{2} \sum_{i,j} J_{ij} \vec{S}_i \cdot \vec{S}_j \ . \tag{3.1}$$

We suppose that $\{\vec{n}_i^{\,0}\}$ is a configuration of unit vectors such that the associated classical energy, $-\frac{1}{2}\sum_{i,j} \hat{J}_{ij} \vec{n}_i^{\,0} \cdot \vec{n}_j^{\,0}$, is a minimum locally. Let, as before, $\vec{a}_i$, $\vec{b}_i$, $\vec{n}_i^{\,0}$ be an orthogonal triad of unit vectors and let $\vec{p}_i^{\,+} = (1/\sqrt{2})(\vec{a}_i + i\vec{b}_i)$, $\vec{p}_i^{\,-} = (1/\sqrt{2}) \times (\vec{a}_i - i\vec{b}_i)$. Then write

$$\begin{aligned} \vec{S}_i &= S_i^a \vec{a}_i + S_i^b \vec{b}_i + S_i^n \vec{n}_i^{\,0} \\ &= \frac{1}{\sqrt{2}} (S_i^a - iS_i^b) \vec{p}_i^{\,+} + \frac{1}{\sqrt{2}} (S_i^a + iS_i^b) \vec{p}_i^{\,-} + S_i^n \vec{n}_i^{\,0} \\ &= \frac{1}{\sqrt{2}} S_i^- \vec{p}_i^{\,+} + \frac{1}{\sqrt{2}} S_i^+ \vec{p}_i^{\,-} + S_i^n \vec{n}_i^{\,0} \ . \end{aligned} \tag{3.2}$$

Now put

$$S_i^n = S - c_i^\dagger c_i + O(S^{-1}) \ ,$$
$$S_i^+ = (2S)^{1/2}[c_i + O(S^{-1})] \ , \qquad (3.3)$$
$$S_i^- (2S)^{1/2}[c_i^\dagger + O(S^{-1})] \ ,$$

or

$$\vec{S}_i = S\vec{n}_i^0 + \sqrt{S}\,(\vec{p}_i^+ c_i^\dagger + \vec{p}_i^- c_i) - c_i^\dagger c_i \vec{n}_i^0 + \cdots \ . \qquad (3.4)$$

The Hamiltonian becomes

$$H = -\tfrac{1}{2}S^2 \sum_{ij} J_{ij}\vec{n}_i^0 \cdot \vec{n}_j^0 - \tfrac{1}{2}S^{3/2}\sum_{ij} J_{ij}(\vec{n}_i^0 \cdot \vec{p}_j^+ c_j^\dagger + \vec{n}_i^0 \cdot \vec{p}_j^- c_j + \vec{n}_j^0 \cdot \vec{p}_i^+ c_i^\dagger + \vec{n}_i^0 \cdot \vec{p}_i^- c_i)$$
$$-\tfrac{1}{2}S\sum_{ij} J_{ij}[(\vec{p}_i^+ c_i^\dagger + \vec{p}_i^- c_i)\cdot(\vec{p}_j^+ c_j^\dagger + \vec{p}_j^- c_j) - \vec{n}_i^0 \cdot \vec{n}_j^0 (c_i^\dagger c_i + c_j^\dagger c_j)] + \text{higher-order terms} \ . \qquad (3.5)$$

Since $\sum_j J_{ij}\vec{n}_j^0 = \lambda_i \vec{n}_i^0$ the linear terms vanish as they should and for the quadratic excitation Hamiltonian we have

$$H_2 = S\Bigg(\sum_i \lambda_i c_i^\dagger c_i - \tfrac{1}{2}\sum_{ij} J_{ij}(\vec{p}_i^+ c_i^\dagger + \vec{p}_i^- c_i)\cdot(\vec{p}_j^+ c_j^\dagger + \vec{p}_j^- c_j)\Bigg) \ . \qquad (3.6)$$

We note that if we were considering the small oscillations of the classical system about an energy minimum we would write

$$\vec{n}_i = \vec{n}_i^0 + \vec{m}_i - \tfrac{1}{2}(\vec{m}_i \cdot \vec{m}_i)\vec{n}_i^0 + \cdots \ ,$$

with

$$\vec{m}_i \cdot \vec{n}_i^0 = 0 \ .$$

Then with

$$\vec{m}_i = \alpha_i \vec{a}_i + \beta_i \vec{b}_i = z_i^- \vec{p}_i^+ + z_i^+ \vec{p}_i^- \ ,$$

where

$$z_i^\pm = (\alpha_i \pm i\beta_i)/\sqrt{2} \ ,$$

the classical quadratic Hamiltonian becomes

$$E_2 = \sum_i \hat{\lambda}_i z_i^+ z_i^- - \tfrac{1}{2}\sum_{i,j}\hat{J}_{ij}(\vec{p}_i^+ z_i^- + \vec{p}_i^- \cdot z_i^+)\cdot(\vec{p}_j^+ z_j^- + \vec{p}_j^- z_j^+) \ . \qquad (3.7)$$

The quantum and classical Hamiltonians are the same in form with the identification $c_i^\dagger \to z_i^-$, $c_i \to z_i^+$, $\lambda_i = S^{-1}\hat{\lambda}_i$, and $J_{ij} = S^{-1}\hat{J}_{ij}$. The z's are to be associated with the two components of circular polarization about $\vec{n}_i^0$. Classically the equation of motion of the $\vec{m}_i$'s is

$$\dot{\vec{m}}_i = \vec{m}_i \times \hat{\lambda}_i \vec{n}_i^0 + \vec{n}_i^0 \times \sum_j \hat{J}_{ij}\vec{m}_j \ . \qquad (3.8)$$

In terms of the α's and β's we then have

$$\dot{\alpha}_i = +\hat{\lambda}_i\beta_i - \sum_j \hat{J}_{ij}[(\vec{b}_i \cdot \vec{a}_j)\alpha_j + (\vec{b}_i \cdot \vec{b}_j)\beta_j] = \frac{\partial E_2}{\partial \beta_i} \ , \qquad (3.9)$$

$$\dot{\beta}_i = -\hat{\lambda}_i\alpha_i + \sum_j \hat{J}_{ij}[(\vec{a}_i \cdot \vec{a}_j)\alpha_j + (\vec{a}_i \cdot \vec{b}_j)\beta_j] = -\frac{\partial E_2}{\partial \alpha_i} \ ,$$

or[24]

$$\dot{z}_i^+ = -i\frac{\partial E_2}{\partial z_i^-} \ , \quad \dot{z}_i^- = i\frac{\partial E_2}{\partial z_i^+} \ . \qquad (3.10)$$

The quantum-mechanical equations of motion are

$$-i\dot{c}_i^\dagger = [H_2, c_i^\dagger] \ \text{ or } \ \dot{c}_i^\dagger = i\frac{\partial H_2}{\partial c_i} \ ,$$
$$-i\dot{c}_i = [H_2, c_i] \ \text{ or } \ \dot{c}_i = -i\frac{\partial H_2}{\partial c_i^\dagger} \ , \qquad (3.11)$$

where the last pair of equalities follows from the boson commutation relations. Thus since H_2 is the same function of $c_i^\dagger$ and c_i as E_2 is of z_i^- and z_i^+, the classical and quantum-mechanical frequencies are equal and the transformation matrices effecting the diagonalization of the energy are also identical. The matrix to be diagonalized is non-Hermitian as is always true in magnon problems. The form of the transformation matrices emerges naturally in the quantum-mechanical formulation.[25] The quantum equations of motion are

$$\dot{c}_i = -i\left(\sum_j P_{ij}c_j^\dagger + \sum_j Q_{ij}c_j\right) \ ,$$
$$\dot{c}_i^\dagger = i\left(\sum_j Q_{ij}^* c_j^\dagger + \sum_j P_{ij}^* c_j\right) \ , \qquad (3.12)$$

where

$$P_{ij}=\hat{\lambda}_i\delta_{ij}-\hat{J}_{ij}(\vec{p}_i^{\,+}\cdot\vec{p}_j^{\,-}) \ , \qquad Q_{ij}=-\hat{J}_{ij}(\vec{p}_i^{\,+}\cdot\vec{p}_j^{\,+}) \ , \tag{3.13}$$

and the asterisk indicates the complex conjugate. If we write c and $c^\dagger$ for the N-component vectors whose components are c_i and $c_i^\dagger$, we have

$$\frac{d}{dt}\begin{vmatrix} c \\ c^\dagger \end{vmatrix}=i\begin{vmatrix} -P & -Q \\ Q^* & P^* \end{vmatrix}\begin{vmatrix} c \\ c^\dagger \end{vmatrix} \ . \tag{3.14}$$

We now make a Bogoliubov transformation to new boson operators, d and $d^\dagger$,

$$c=g^*d+fd^\dagger \ , \quad c^\dagger=f^*d+gd^\dagger \ , \tag{3.15}$$

where g and f are $N\times N$ matrices. If the boson commutation rules are preserved

$$g^*f^T-fg^\dagger=0 \ , \quad g^*g^T-ff^\dagger=1 \ ,$$

or

$$\begin{vmatrix} g^* & f \\ f^* & g \end{vmatrix}\begin{vmatrix} -1 & 0 \\ 0 & +1 \end{vmatrix}\begin{vmatrix} g^* & f \\ f^* & g \end{vmatrix}^\dagger=\begin{vmatrix} -1 & 0 \\ 0 & +1 \end{vmatrix} \ . \tag{3.16}$$

From this it follows that

$$\begin{vmatrix} g^* & f \\ f^* & g \end{vmatrix}^{-1}=\begin{vmatrix} g^T & -f^T \\ -f^\dagger & g^\dagger \end{vmatrix} \ . \tag{3.17}$$

If the new variables are to diagonalize H_2 then we require

$$\frac{d}{dt}\begin{vmatrix} d \\ d^\dagger \end{vmatrix}=i\begin{vmatrix} -\Omega & 0 \\ 0 & \Omega \end{vmatrix}\begin{vmatrix} d \\ d^\dagger \end{vmatrix} \ , \tag{3.18}$$

where Ω is *the diagonal matrix of eigenfrequencies.* We therefore must have

$$\frac{d}{dt}\begin{vmatrix} g^* & f \\ f^* & g \end{vmatrix}\begin{vmatrix} d \\ d^\dagger \end{vmatrix}=i\begin{vmatrix} g^* & f \\ f^* & g \end{vmatrix}\begin{vmatrix} -\Omega & 0 \\ 0 & \Omega \end{vmatrix}\begin{vmatrix} d \\ d^\dagger \end{vmatrix}=i\begin{vmatrix} -P & -Q \\ Q^* & P^* \end{vmatrix}\begin{vmatrix} g^* & f \\ f^* & g \end{vmatrix}\begin{vmatrix} d \\ d^\dagger \end{vmatrix} \ ,$$

so that

$$\begin{vmatrix} g^* & f \\ f^* & g \end{vmatrix}\begin{vmatrix} -\Omega & 0 \\ 0 & \Omega \end{vmatrix}=\begin{vmatrix} -P & -Q \\ Q^* & P^* \end{vmatrix}\begin{vmatrix} g^* & f \\ f^* & g \end{vmatrix} \ , \tag{3.19}$$

or if ν labels the eigenvalues

$$f_{i\nu}\Omega_\nu=-\sum_j P_{ij}f_{j\nu}-\sum_j Q_{ij}g_{j\nu} \ , \qquad g_{i\nu}\Omega_\nu=\sum_j Q_{ij}^*f_{j\nu}+\sum_j P_{ij}^*g_{j\nu} \ . \tag{3.20}$$

If we compare these equations with the classical ones we find that they are identical with the latter if $f_i=z_i^+$ and $g_i=z_i^-$. Now that the restrictions enforced on f and g, Eq. (3.16), by the commutation relations have been found, it will be convenient to employ the notation z_i^+ and z_i^- [Eq. (3.7)] in place of f_i and g_i. Rewriting Eq. (3.16) in these variables we obtain the appropriate orthogonality and normalization relations for the classical modes

$$\sum_i(z_{i\nu}^+z_{i\nu'}^--z_{i\nu}^-z_{i\nu'}^+)=0 \ , \qquad \sum_i(z_{i\nu}^-z_{i\nu'}^{-*}-z_{i\nu}^+z_{i\nu'}^{+*})=\delta_{\nu\nu'} \ . \tag{3.21}$$

It may be remarked that one can verify readily that, if the energy matrix (see Sec. II) has no negative eigenvalues, thus guaranteeing the existence of an energy minimum, then all the frequencies Ω_ν are real.

We may now write down expressions for the energy and for the magnetization of the system. Replacing the $c_i^\dagger$ and c_i in H_2 by their expansions in the $d_\nu^\dagger$'s and d_ν's one finds

$$H_2=-\tfrac{1}{2}\sum_i\lambda_i+\sum_\nu(n_\nu+\tfrac{1}{2})\Omega_\nu \ , \tag{3.22}$$

where

$$n_\nu=d_\nu^\dagger d_\nu \ .$$

The zero-point energy is $-\frac{1}{2}\sum\lambda_i+\frac{1}{2}\sum\Omega_\nu$, which may be manipulated into a form which shows that it is negative as it should be. The spin deviation operator at site i is $c_i^\dagger c_i$. This is not diagonal, but its expectation value is

$$\langle c_i^\dagger c_i\rangle=\sum_\nu(|z_{i\nu}^+|^2\langle n_\nu+1\rangle+|z_{i\nu}^-|^2\langle n_\nu\rangle) \ ,$$

with $\langle n_\nu\rangle$ the expectation value of $d_\nu^\dagger d_\nu$. The mean spin deviation for all sites is

$$\frac{1}{N}\sum_i\langle c_i^\dagger c_i\rangle=\sum_\nu|z_{i\nu}^+|^2+\sum_\nu\langle n_\nu\rangle\sum_i(|z_{i\nu}^+|^2+|z_{i\nu}^-|^2) \ , \tag{3.23}$$

the first term being the zero-point spin reduction and the latter the thermally dependent part. The ground-state wave function can be found by a technique familiar in ordered systems.[24] If $|G\rangle$ is this wave function it satisfies the equations

$$d_\nu|G\rangle=0$$

or

$$\sum_i[(z^{-T})_{\nu i}c_i-(z^{+T})_{\nu i}c_i^\dagger]|G\rangle=0 \ .$$

Since $|G\rangle$ consists of excitations from the original classical ground state, $|C\rangle$ (with $c_i|C\rangle=0$), it may

be written

$$|G\rangle = F(c^\dagger)|C\rangle$$

and then we have

$$\sum_i (z^{-T})_{\nu i} \frac{\partial F}{\partial c_i^\dagger} = \left(\sum_i (z^{+T})_{\nu i} c_i^\dagger \right) F$$

and

$$F = \exp\left(\sum_{ij} c_i^\dagger [(z^{-T})^{-1}(z^{+T})]_{ij} c_j^\dagger \right) .$$

It would be possible to study the nature of the ground state in some detail by examining the magnitude of the pair-flipping matrix elements $[(z^{-T})^{-1}(z^{+T})]_{ij}$. This state, like other magnon ground states, contains a nonphysical component, consisting of excitations out of the manifold of real spin states.

IV. COMPUTED SPECTRA AND COMPARISON WITH EXPERIMENT

In this section we present and discuss a number of examples of excitation frequency spectra computed by solving Eq. (3.9) or a generalized version thereof for simulated systems of spins. The cases have been chosen to illustrate a wide variety of properties and effects. For example, Alloul[26] and Monod and Préjean[27] have carried out experiments demonstrating the presence of anisotropy energy in dilute *Cu*Mn. Accordingly, we have examined the effect of various types of anisotropy on the frequency spectra and give a preliminary account of our results in Sec. IV B.

A. Spectra with purely isotropic exchange

Equations (3.9) have been solved for EC's corresponding to two series of ten spatial distributions of 96 spins each, one series with $c = 0.3$ at.% and one with $c = 0.9$ at.%. The structure of the mode distribution varied relatively little from one 96-spin case to the next, consisting of two zero-frequency modes followed by a low-lying peak in the mode density. At the top of the spectrum one always finds a set of modes at a frequency approximately twice the nearest-neighbor coupling strength. These are easily identified as nearest-neighbor pair modes. In plotting the spectra (Fig. 9) we show only the low-frequency portion of primary interest. Further, the three modes which are related to the rotational symmetry of the system (see Appendix) have been removed from the spectrum, since they are apparently unrelated to the thermodynamics of a macroscopic spin-glass. The spectra in Fig. 9 are plotted on frequency scales differing by a factor of 3 to illustrate the scaling effect with concentration. The spectral width is seen to vary linearly with c (as expected) within statistical error. Higher-frequency modes associated with identifiable pairs and close-neighbor clusters do not, of course, scale.

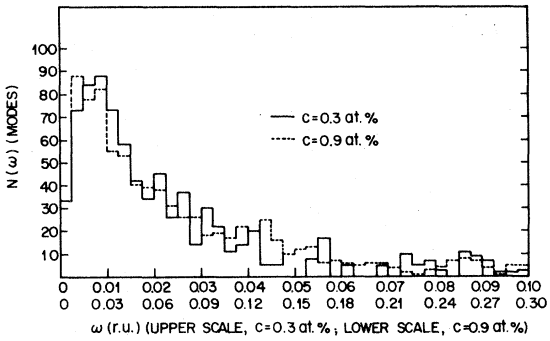

FIG. 9. Elementary excitation frequency spectra for two sets of ten spatial distributions of $N = 96$ spins at $c = 0.3$ at.% and 0.9 at.%, respectively. The abscissas are scaled by $\times 3$ to make the spectra coincide, illustrating the RKKY scaling effect.

Since the foregoing results were published,[8] additional spectra have been obtained with simulations using $N = 172$ spins, permitting us to examine the dependence, if any, on N and to scrutinize the low-frequency portion of the spectrum. Results are shown in Fig. 10 using a histogram interval half that of Fig. 9. The general shape and width of the spectrum in Fig. 10 is the same as before, suggesting that either size of sample gives a good approximation to a macroscopic system (except at the lowest frequencies as discussed in Sec. IV C). The additional detail near $\omega = 0$ shows the mode density dropping sharply toward zero at $\omega \to 0$. It is necessary that this should happen if the ground state is to be stable in the spin-wave approximation, since the mean spin deviation given by Eq. (3.23) diverges at finite T if $N(\omega) > 0$ as $\omega \to 0$. This drop in $N(\omega)$ is responsible for the

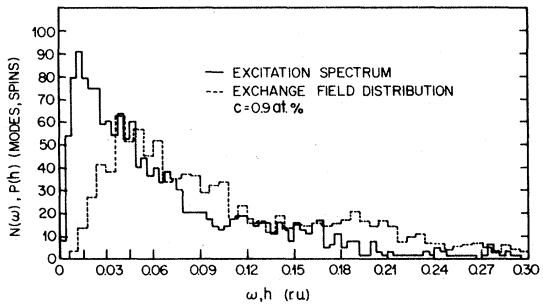

FIG. 10. Excitation spectrum $N(\omega)$ for $c = 0.9$ at.% derived from seven spatial distributions of $N = 172$ spins each (solid line). Distribution $P(h)$ of exchange fields from EC's for 10 distributions of 177 spins each at $c = 0.9$ at.%, normalized to the same total area as $N(\omega)$ (dashed curve).

fact that experimental specific-heat curves $C_M(T)$ are not linear at $T \to 0$, but vary as higher powers of T. The variation of $N(\omega)$ as $\omega \to 0$ is not inconsistent with the form $N(\omega) \cong D\omega^2$ which results from the linear dispersion law[6] for long-wavelength excitations. The finite sample size precludes a more precise statement on this matter.

For comparison in Fig. 10 we also show (dashed curve) a distribution of exchange fields for ordered spins at this concentration. It is clear from the striking contrast between $P(h)$ and $N(\omega)$ at low energies that a specific heat calculated on the basis of single-particle excitations [from $P(h)$] would be drastically different at low temperatures from that derived from $N(\omega)$.

The elementary excitations of magnetic systems with crystalline order are states which extend over the entire sample. It is interesting to inquire whether extended states are also present in spin-glasses, as would be suggested by the cooperative nature of the spin-glass transition. We probe this question by studying a form of localization index for the modes μ

$$L_\mu = \sum_i W_{i\mu}^2 \Big/ \left(\sum_i W_{i\mu} \right)^2 , \tag{4.1}$$

where

$$W_{i\mu} = |\alpha_{i\mu}|^2 + |\beta_{i\mu}|^2$$

is a weight coefficient for mode μ; $W_{i\mu}$ is actually the time average value of $\vec{m}_i \cdot \vec{m}_i$, where $\vec{m}_i$ is the displacement of spin i from equilibrium [see Eq. (2.4)]. L_μ will vary from a value of unity for a completely localized mode to a value of order N^{-1} for a mode which involves the entire system. A plot of L_μ values versus ω for a system of 96 spins at $c = 0.9$ at.% is shown in Fig. 11. A distinct trend in L_μ values is noted, starting from $L_\mu \sim 0.5$ for pair modes at the top of the spectrum to strongly extended modes ($L_\mu \sim N^{-1}$) at the lowest frequencies. Visual examination of the lowest modes failed to reveal any wavelike character. Ching *et al.*[9] have examined the excitation spectra of finite simulations for wavelike behavior using several model interaction laws by calculating dynamic-structure factors. Such modes, if they exist, are apparently beyond the spatial resolution of the finite systems investigated.

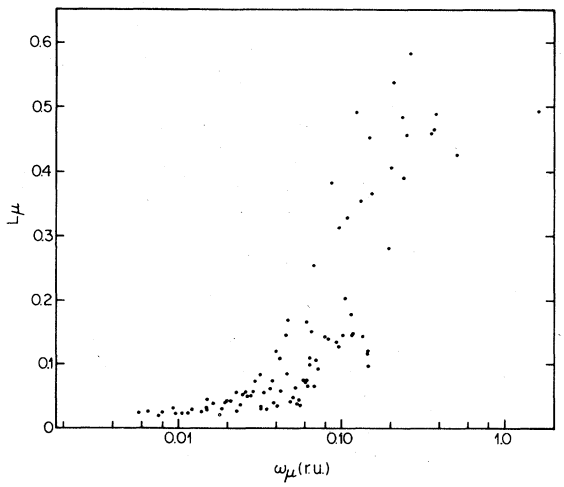

FIG. 11. Plot of localization indices L_μ calculated with Eq. (4.1) vs mode frequency ω_μ for a system of 96 spins at $c = 0.9$ at.%.

For the success of the spin-wave-type approximation employed here it is necessary for the ground state to be stable. One measure of its stability is the extent of zero-point fluctuation in the magnetization as reflected by the zero-temperature value of the spin deviation in Eq. (3.23). This quantity has been evaluated for the same mode distribution used in Fig. 11 to give

$$N^{-1} \sum_i \langle c_i^* c_i \rangle \sim 0.15 , \tag{4.2}$$

which is a reduction by $\sim 6\%$ for an $S = \frac{5}{2}$ system such as Mn in Cu. This is a reduction comparable to that of two-dimensional crystalline antiferromagnets, and is a sign of good stability in the ground configuration. Substantially larger reductions at some sites could, however, be concealed in the average in Eq. (4.2). For $S = \frac{1}{2}$, however, the deviation would be $\sim 30\%$ and the ground state is therefore very "mushy." Klemm[28] has argued that spin-glass ordering is not possible for $S = \frac{1}{2}$. We have also calculated the quantum correction to the ground-state energy given by Eq. (3.22) (with $\langle n_\nu \rangle = 0$) for the same case. This is

$$\Delta E = \tfrac{1}{2} \sum_\nu \Omega_\nu - \tfrac{1}{2} \sum_i \hat{\lambda}_i = -0.75 , \tag{4.3}$$

expressed in reduced units, to be compared with the classical energy [Eq. (2.1)]

$$E_0 = -\tfrac{1}{2} \sum_{i,j} \hat{J}_{ij} \vec{n}_i^{\,0} \cdot \vec{n}_j^{\,0} = -11.66 , \tag{4.4}$$

again in ru. ΔE is negative as expected. To compare ΔE with E_0 for a system of spins S we note that ΔE is multiplied by S (Ref. 19) and E_0 by S^2 [Eq. (3.15)]. Again, the zero-point correction is modest for spins $S = \frac{5}{2}$.

B. Effects of various additional interaction terms on the frequency spectra

It is important to ascertain the effect of various modifications of the interactions on the frequency spectra, even though such changes are small compared with the RKKY exchange. Thus, we have investigated how the results are changed by two forms of anisotropy, dipolar and local (cubic), and by an ap-

plied field. We further studied the effect of damping of the RKKY interaction. Inclusion of these effects modifies the equilibrium condition [Eq. (2.2)] and equations of motion [Eq. (3.9)], so we begin by stating these relations with all effects included. We work throughout in reduced units.[20,29] The equilibrium condition becomes

$$\vec{n}_i^{\,0}\hat{\lambda}_i = \vec{h}_0 + \sum_j \hat{J}_{ij}\vec{n}_j^{\,0} + d\sum_j [\vec{n}_j^{\,0} - 3\vec{u}_{ij}(\vec{n}_j^{\,0}\cdot\vec{u}_{ij})]r_{ij}^{-3} + \Delta_c[\vec{i}\,(n_{ix}^0)^3 + \vec{j}\,(n_{iy}^0)^3 + \vec{k}\,(n_{iz}^0)^3] \quad , \tag{4.5}$$

where $\vec{h}_0$ is the applied field, $d = D/A$, where $D = (g\mu_B S)^2$ is the dipolar coefficient, $\vec{u}_{ij}$ is the unit vector $\vec{r}_{ij}/r_{ij}$, and Δ_c is the cubic anisotropy parameter. The cubic anisotropy energy is given by

$$E_c = -\tfrac{1}{4}\Delta_c \sum_i [(n_{ix})^4 + (n_{iy})^4 + (n_{iz})^4] \quad .$$

The corresponding equations of motion, using Cartesian representation of the spin displacements [Eq. (3.9)], are

$$\dot{\alpha}_i = -3\Delta_c\alpha_i[a_{ix}b_{ix}(n_{ix}^0)^2 + a_{iy}b_{iy}(n_{iy}^0)^2 + a_{iz}b_{iz}(n_{iz}^0)^2]$$
$$+\beta_i\left[\vec{n}_i^{\,0}\cdot\left(\vec{h}_0 + \sum_j \hat{J}_{ij}\vec{n}_j^{\,0}\right) + \Delta_c\{(n_{ix}^0)^4 + (n_{iy}^0)^4 + (n_{iz}^0)^4 - 3[(b_{ix}n_{ix}^0)^2 + (b_{iy}n_{iy}^0)^2 + (b_{iz}n_{iz}^0)^2]\}\right]$$
$$+d\sum_j r_{ij}^{-3}[\alpha_j(\vec{b}_i\cdot\vec{a}_j - 3\vec{b}_i\cdot\vec{u}_{ij}\vec{a}_j\cdot\vec{u}_{ij}) + \beta_j(\vec{b}_i\cdot\vec{b}_j - 3\vec{b}_i\cdot\vec{u}_{ij}\vec{b}_j\cdot\vec{u}_{ij})] - \sum_i \hat{J}_{ij}(\alpha_j\vec{b}_i\cdot\vec{a}_j + \beta_j\vec{b}_i\cdot\vec{b}_j) \quad , \tag{4.6a}$$

$$\dot{\beta}_i = \alpha_i\left[\Delta_c\{3[(a_{ix}n_{ix}^0)^2 + (a_{iy}n_{iy}^0)^2 + (a_{iz}n_{iz}^0)^2] - (n_{iz}^0)^4 - (n_{ix}^0)^4 - (n_{iz}^0)^4\} - \vec{n}_i^{\,0}\cdot\left[\vec{h}_0 + \sum_j \vec{J}_{ij}\vec{n}_j^{\,0}\right]\right]$$
$$+3\Delta_c\beta_i[a_{ix}b_{ix}(n_{ix}^0)^2 + a_{iy}b_{iy}(n_{iy}^0)^2 + a_{iz}b_{iz}(n_{iz}^0)^2] + \sum_j \hat{J}_{ij}(\alpha_j\vec{a}_i\cdot\vec{a}_j + \beta_j\vec{a}_i\cdot\vec{b}_j)$$
$$-d\sum_j r_{ij}^{-3}[\alpha_j(\vec{a}_i\cdot\vec{a}_j - 3\vec{a}_i\cdot\vec{u}_{ij}\vec{a}_j\cdot\vec{u}_{ij}) + \beta_j(\vec{a}_i\cdot\vec{b}_j - 3\vec{a}_i\cdot\vec{u}_{ij}\vec{b}_j\cdot\vec{u}_{ij})] \quad . \tag{4.6b}$$

Particular cases from Eqs. (4.5) and (4.6) will now be discussed in turn.

1. *Effect of RKKY damping*

As mentioned in the Introduction, there is a possibility that self-damping effects on the RKKY oscillations may be important for concentrations of magnetic ions even as low as $c \sim 1$ at.%. On the de Gennes model[30] this damping is asymptotically exponential; this form has been adopted in the present work. To investigate the effect this has on the frequency spectrum, we compare a 96-spin $c = 0.9$ at.% spectrum without damping with spectra calculated with two levels of exponential damping in Fig. 12. There we plot individual mode frequencies with damped RKKY against the same mode frequency without damping. The result is a striking one in that modes in the low-frequency peak of the spectrum are simply scaled to lower frequencies by the factors 0.89 and 0.67 in the cases considered. The exponential damping lengths, $r_0 = 28.5a$ and $8.41a$ shown in the figure were chosen

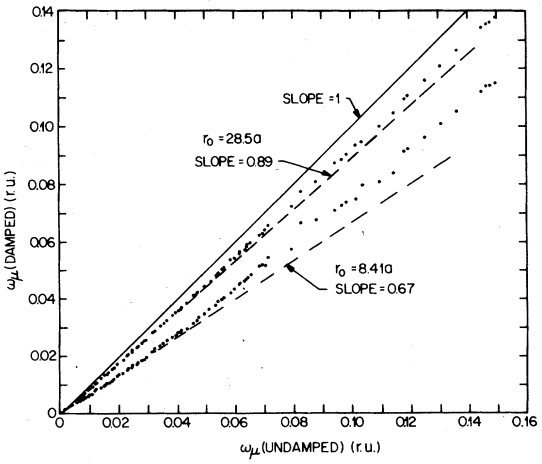

FIG. 12. Plot of mode frequencies ω_ν (DAMPED) vs ω_ν (UNDAMPED) for corresponding modes for a distribution of 96 spins at $c = 0.9$ at.%. The damping lengths r_0 employed are shown with the resulting asymptotic ($\omega_\nu \to 0$) slopes.

to correspond to narrowing of the distributions of exchange field components [e.g., $P(h_z)$] by 10% and 30%, respectively.[12] The effect of damping on the spin-glass frequency spectra is seen to consist of narrowing by the same amount with very little change in shape. The higher-frequency modes are affected more weakly. This is to be expected, since the stronger RKKY fields are changed less by the damping. It is also clear from these results that the shape of the low-frequency peak in the spectrum (Fig. 10) is not uniquely related to the long-range character of the RKKY interaction. Indeed, the EA model interaction yields a similar spectral shape.[9] These results are used in Sec. IV C to discuss the concentration dependence of the specific heat and the spin-glass ordering temperature.

2. *Dipolar anisotropy*

When dipolar interactions are added to the RKKY exchange, the rotational symmetry is broken and the spins now take on a preferred orientation relative to the crystal axes. A full study of the behavior of this model in the presence of anisotropy is under way and only a preliminary report on the resulting spectra will be given here. The classical dipolar field at site i is stated in the equilibrium equation (4.5). The classical coefficient D is rather small compared with RKKY exchange, having a ratio $D/A \sim 5\times10^{-4}$ for dilute CuMn. Fields of this magnitude were found to have a negligible effect on the computed frequency spectrum.

To consider the electron-spin analog of pseudodipolar coupling[31] we have also studied dipolar interactions of the form given in Eq. (4.5) but with bigger coefficients. To obtain these spectra the spins were first equilibrated using Eq. (4.5), then the frequencies were obtained with Eqs. (4.6a) and (4.6b). Results are shown in Fig. 13 for $d=0.002$ and 0.01, where mode frequencies with dipolar coupling added are plotted against those with exchange alone. In this and subsequent plots of this nature it is assumed that no mode crossing occurs. Breakdown of this assumption would result in some artificial "smoothing" of the resulting curves, but would not alter the general trend. For the smaller d value in Fig. 13 (~ 4 times the classical dipolar value) there is a small increase in frequencies below $\omega \sim 0.02$ such as to introduce a small zero-frequency gap in the spectrum. The effect essentially disappears above $\omega \sim 0.02$. For D/A five times larger the gap effect is considerably greater and extends over about twice the frequency range. Again, it collapses quite abruptly above an upper limit $\omega \sim 0.04$.

The foregoing results bear a qualitative similarity to the effect of anisotropy on the spin-wave spectrum of a simple antiferromagnet, i.e., a large effect at the bottom of the spectrum which diminishes to zero at higher frequencies. However, we see no obvious reason for the abrupt high-frequency cutoff found here. We might add that these results are changed only slightly and in an unexpected way by truncating the dipolar coupling range. Truncation to zero beyond the third-neighbor shell for $D/A=0.02$ was found only to *increase* slightly the frequency shift of the lowest half dozen modes or so, the effect diminishing rapidly with frequency.

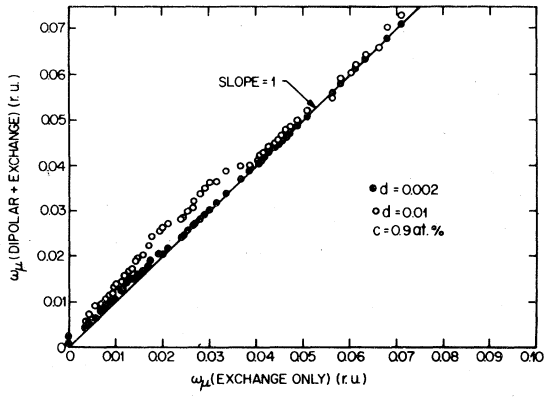

FIG. 13. Plot of mode frequencies ω_ν with dipolar coupling magnitude shown against corresponding frequencies with exchange alone. A line of unit slope is drawn for comparison.

3. *Single-ion cubic anisotropy*

A similar study to that described in Sec. IV B 2 has been carried out for the case of purely cubic single-

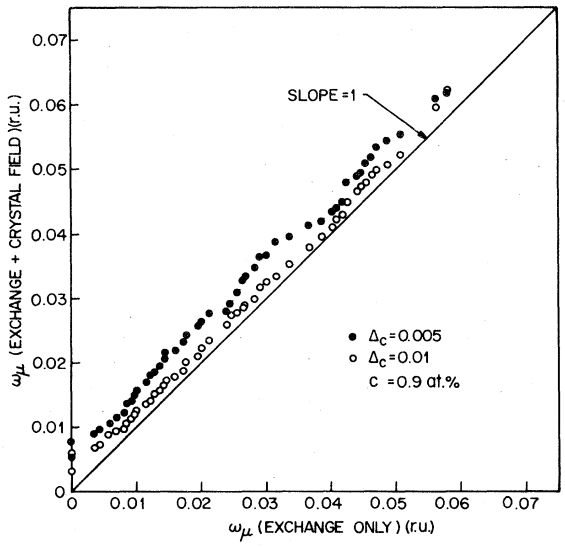

FIG. 14. Plot of mode frequencies ω_ν with cubic crystal-field anisotropy as shown (units of $2\sqrt{2}A/a^3$) against corresponding frequencies with exchange alone. A line of unit slope is drawn for comparison.

ion anisotropy energy as embodied in Eqs. (4.5) and (4.6). The results are shown in Fig. 14, in the same format as in Fig. 13, using crystal-field coefficients $\Delta_c = 0.005$ and 0.01 units of $2\sqrt{2}A/a^3$. Unlike the dipolar terms, crystal-field anisotropy has the effect of producing an approximately uniform frequency increase of $0.5\Delta_c$ over the frequency range in the figure. There are also noticeable nonlinearities in many instances. At higher frequencies the effect of Δ_c diminishes. It is interesting to note that the detailed peaks and valleys in the shift effect of Figs. 13 and 14 (for the larger values of d and Δ_c) are quite similar for these two rather disparate forms of anisotropy. Further, it is not surprising that the effect of Δ_c on the spectrum is more global than that of d, because Δ_c affects all spins whereas there may be many loosely coupled spin clusters with very small dipolar anisotropy.

4. *Applied uniform field*

Finally, we exhibit the low-frequency portion of two spectra obtained in applied fields $h_0 = 0.005$ and 0.01 in Fig. 15. Again, the frequencies with h_0 present are plotted against those found with exchange alone. Below $\omega = 0.035$ one finds an approximately uniform increase in frequency which appears to be somewhat nonlinear in h_0. Individual modes are found to vary in a strongly nonlinear fashion. At higher frequencies the field effect is essentially random in sign and again highly nonlinear. Since $h_0 = 0.01$ corresponds to roughly 35 kG from *Cu*Mn at this concentration, these results suggest that the specific heat in this case would be only slightly modified by laboratory fields of this magnitude. Of the two zero-frequency modes noted in the Appendix, one remains at zero for all h_0; the other is equal to h_0 in frequency and is the EPR mode of the system.

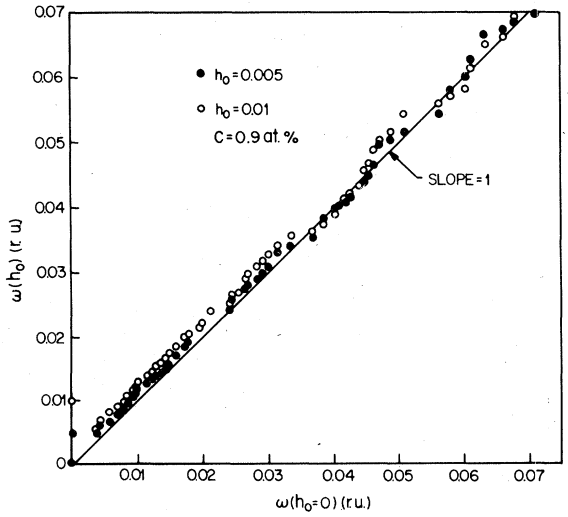

FIG. 15. Plot of mode frequencies ω_ν in fields h_0 as shown against corresponding frequencies in zero field. A line of unit slope is drawn for comparison.

C. Specific heat

Since our initial report on this work,[8] comprehensive results for the magnetic specific heat C_M of *Cu*Mn spin-glass have been reported by Fogle *et al.*[32] and by Martin.[33] These new data not only give the detailed variation of C_M throughout the ordered temperature region, they also provide a reasonably complete account of the concentration dependence. It has been noted[32,33] that the results do not obey the scaling law $[C_M/c = f(T/c)]$ expected for a system with an r^{-3} interaction potential. We address ourselves to this question below, and, in particular, seek an explanation in terms of self-damping of the RKKY oscillations.[12] Larsen[34] has incorporated self-damping into the Edwards-Anderson model[1] expression for the ordering temperature T_G in an effort to understand the failure of T_G to obey scaling laws. Our approach is based on the results of Sec. IV B *1*. The specific-heat data of Refs. 32 and 33 are in good accord with one another and with eariler results of Wenger and Keesom.[35] In the discussion below, we shall make use of the convenient numerical representation of specific-heat data given by Martin[33] for *Cu*Mn and the results of Wenger and Keesom for *Au*Fe.[36]

It should be emphasized that the use of the data we have gathered on the excitations to calculate specific heat is an exploratory exercise. Since we do not know the range of validity of the analysis which yields the modes, it is clearly not possible to estimate a temperature range over which one may legitimately do thermodynamics. So we are, in effect, exploring the consequences of assuming the theory valid.

The specific heat $C_M(T)$ for 0.88 at.% Mn in Cu was evaluated from our model assuming Bose occupation factors for the elementary excitations, which were assumed to be distributed according to the histogram in Fig. 10. C_M can then be written

$$C_M = N_0 c k_B T_r \sum_{m=1}^{\infty} f_m \sum_{l=1}^{\infty} (F_{lm-1} - F_{lm}) \Big/ l^2 \quad , \qquad (4.7)$$

where N_0 is Avogadro's number, T_r is the (reduced) temperature in units of the histogram interval, f_m is the fraction of calculated mode frequencies which occur in the mth histogram interval, and

$$F_{lm} = (m^2 l^2/T_r^2 + 2ml/T_r + 2)\exp(-ml/T_r) \quad .$$

Noting that C_M is a function only of T_r and the f_m's we have fitted Eq. (4.7) to the specific-heat data of Martin[33] by adjusting the RKKY constant A which

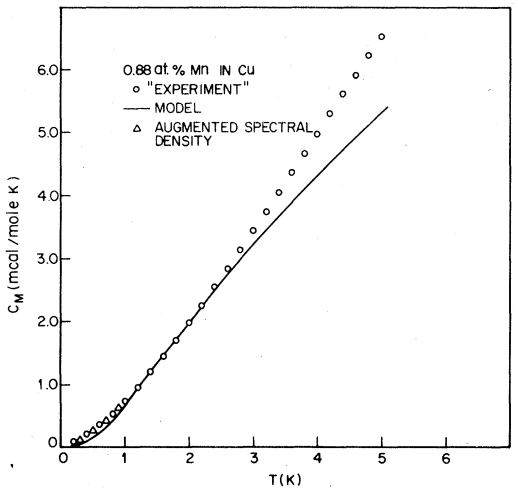

FIG. 16. Plot of both "experimental" specific-heat data (from numerical representation of data in Ref. 33) and model calculations as described in the text for 0.88 at.% Mn in Cu.

defines the T_r scale. For this purpose we use as a guide the experimental measurements by Smith.[37] The fit shown in Fig. 16 is obtained using $A = 1.02 \times 10^{-36}$ erg cm^3, which is 15% smaller than the value $A = 1.20 \times 10^{-36}$ erg cm^3 derived from Smith's data.[37] The size and direction of this discrepancy is not surprising in view of the self-damping effects to be discussed below.

Regarding Fig. 16 we note that the model calculation underestimates C_M at the lowest temperature, followed by a region of good agreement, then falls below experiment for $T > 3$ K. Since $T_G \sim 10$ K for this concentration, our spin-wave type of model is apparently valid up to some temperature $T \sim 0.3 T_G$. The discrepancy below 1 K is more interesting, however, and presumably arises from a defect in the calculated spectrum stemming from the finite size of our simulation volume. Such a finite volume is expected to distort the spectrum by attenuating the density of very low-frequency modes whose wavelength will not fit into its dimensions. Assuming linear dispersion[6] and taking a rough estimate for the constant ω/k[38] one finds that for frequencies in the middle of the first histogram interval (Fig. 10) the wavelength is greater than the simulation cube dimension. This strongly suggests that the number of modes in that lowest interval is underestimated. Accordingly, we have also calculated $C_M(T)$ assuming one additional mode per 172-spin sample in the lowest interval. The results are shown in Fig. 16 (augmented spectral density) and are seen to be in significantly better agreement with experiment.

In calculating $C_M(T)$ for $0 \leq T \leq 3$ K one might question the validity of Eq. (4.7) since the histogram interval itself is nearly 2 K. We examined this point by recalculating $C_M(T)$ using a parabolic representation for the mode density over the first two histogram intervals. The results were only distinguishable from those in Fig. 16 at $T < 1$ K, where the difference was also very small.

Further calculations show that introduction of an energy gap in the spectrum such as is caused by dipolar or cubic anisotropy (Secs. IV B *2* and IV B *3*) causes the agreement with experiment to deteriorate. The results are consistent, of course, with the presence of the classical dipolar interaction because of its negligible effect on the spectrum. From the results in Fig. 14 we can state that cubic anisotropy present must satisfy $\Delta_c/k_B < 1$ K. To our knowledge there are no published measurements of $C_M(T)$ with $T \ll T_G$ for *Cu*Mn in an applied magnetic field.

Before considering the concentration dependence of $C_M(T)$, we present in Fig. 17 a comparison of model calculations with experimental specific-heat results for 1 at.% Fe in Au.[36] The model curve corresponds to $A = 1.20 \times 10^{-36}$ erg cm^3, the value for 0.1 at.% Mn in Cu given by Smith.[37] To our knowledge there are no experimental data on A for *Au*Fe. There are striking differences between the *Au*Fe and the *Cu*Mn cases, most likely resulting from the fact that Fe impurities in Au undergo Kondo condensation at $T_K \sim 0.5$ K.[13] As a result, the excitation spectrum of AuFe probably tends to collapse to lower frequencies as T approaches T_K from above. Thus, one finds a more nearly linear behavior of $C_M(T)$ as $T \to 0$ than the present model can explain. The apparently good agreement between model and experiment at higher T (Fig. 17) must not be taken seriously without an independent measure of A for this case.

Martin[33] has noted that experimental curves for

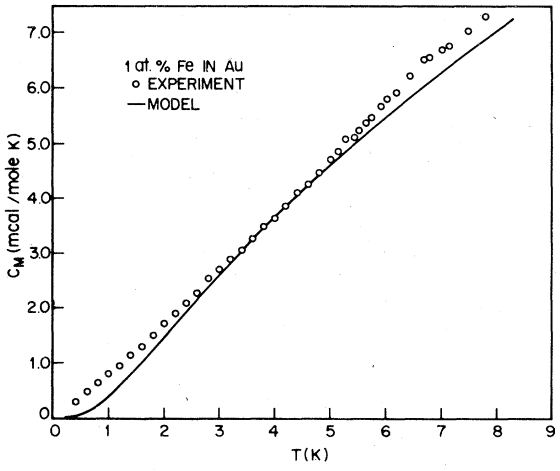

FIG. 17. Plot of experimental specific heat for 1 at.% Fe in Au from Ref. 36 with model calculation curve fitted as described in text.

$C_M(T)$ do not scale correctly with concentration c. In fact, they behave as though A were decreasing significantly with increasing c for $c \sim 1$ at.%. The spin-glass ordering temperature T_G also deviates[13] from the scaling law $T_G \propto c$ in this concentration range. It is very likely that both effects are caused by self-damping of the RKKY exchange oscillations. The importance of self-damping in these systems has been pointed out.[12,34] We shall combine the results of Ref. 12 with the RKKY damping studies of Sec. IV B *1* to examine the magnitude and concentration dependence of these effects. The half-width (HW) of the distribution of any RKKY field component[12] has been found to vary as $\mathrm{HW} \propto \exp(-1.59 N_{r_0}^{-1/3})$, where $N_{r_0} = \frac{4}{3}\pi\rho c r_0^3$ is the average number of magnetic impurities within a sphere of radius r_0, the exponential damping length and ρ is the volume density of available impurity sites. Since the scale of the frequency spectrum was found to vary (Sec. IV B *1*) in nearly the same way with r_0 as the half-width above, we may express

$$A_{\mathrm{eff}}(r_0) = A \exp(-1.75 N_{r_0}^{-1/3}) \ , \tag{4.8}$$

where A_{eff} is the effective value of the RKKY constant. When the damping is caused by the magnetic impurities themselves, one has $r_0^{-1} \propto c$ and[12]

$$A_{\mathrm{eff}}(c) = A \exp[-1.77(\rho c)^{2/3}\sigma_{\mathrm{Mn}} n] \ , \tag{4.9}$$

where σ_{Mn} is the appropriate scattering cross section and n is the number of conduction electrons per atom. We use the scaled temperature value T/c at which the scaled specific heat C_M/c in Martin's Fig. 6 (Ref. 33) equals a typical value (0.35 cal/K g atom Mn) as a measure of $A_{\mathrm{eff}}(c)$. In Fig. 18 these quantities are plotted semilogarithmically against $c^{2/3}$ and are seen to be consistent with the functional form of Eq. (4.9). In the same figure we also plot the variation of experimental T_G values[39] for *Cu*Mn relative to the linear variation at low concentrations given by $[1.87(c/1\ \mathrm{ppm}) + 6.6] \times 10^{-3}$ K as reported by Hirschkoff *et al.*[40] In Fig. 18 T_G is seen to vary in a manner similar to the scaled temperatures.[41]

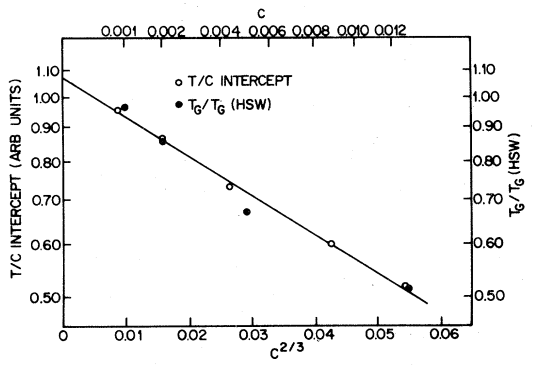

FIG. 18. Plot of relative values of A_{eff} as measured (i) by the T_c intercept value with specific heat (Ref. 33) described in the text and (ii) by experimental T_G values relative to the low-concentration variation T_G (HSW) given in Ref. 40. These data are plotted against $c^{2/3}$ [see Eq. (4.9)].

We conclude that the deviation from scaling in *Cu*Mn is consistent with the self-damping mechanism. From the slope of the line drawn in Fig. 18 and Eq. (4.9) one finds the value $\sigma_{\mathrm{Mn}} = 3.1a^2$, which is considerably larger than the resistivity value $\sigma_r = 0.54a^2$.[12] There is evidence that the RKKY damping cross section for Al in Cu (Ref. 12) is also considerably larger than the resistivity value. Finally, it is interesting to note that the measurements of RKKY coupling in Ref. 37 show a concentration dependence consistent with the results in Fig. 18. The 15% discrepancy between A_{eff} as derived at $c = 0.88$ at.% from $C_M(T)$ and the value in Ref. 37 obtained at $c < 0.1$ at.% is at least in qualitative accord with the present arguments. Using the straight line drawn in Fig. 18 and taking the specific-heat value 1.02×10^{-36} erg cm^3 as A_{eff} in Eq. (4.8), we deduce $A = 1.82 \times 10^{-36}$ erg cm^3 for an isolated pair of Mn impurities.

D. Zero-temperature susceptibility

Previous theories of the magnetic response of spin-glass systems have been based on a picture combining the molecular-field distribution $P(H)$ for bulk, reversible magnetization with a model of magnetic "monodomains"[13,42] consisting of n spins each with a magnetic moment $\mu \propto \sqrt{n}$. In considering the small-field reversible[13] ("first-magnetization"[42]) susceptibility both the bulk-polarization and domain-rotation contributions would have to be considered. However, there is some question about the domain contribution because of recent evidence presented by Alloul[26] that there are no such domains in a zero-field cooled sample. We shall comment further on this question in our discussion below. We present in this section a computation, based on our model, of the bulk-polarization contribution to $\chi^r(0)$. $\chi^r(0)$ was measured by Careaga *et al.*[42] The bulk contribution will be calculated here both by perturbation theory and by measuring the response to an applied field in the simulation.

To calculate the magnetic response of a system of N spins to a small applied dc field $\vec{H}_0$ one adds a term $-g\mu_B H_0 \sum_i S_{zi}$ to the Hamiltonian [Eq. (3.1)]. The classical equilibrium condition [Eq. (4.5)] may be reexpressed as

$$\vec{n}_i \times \left[\vec{h}_0 + \sum_j \hat{J}_{ij}\vec{n}_j\right] = 0 \ . \tag{4.10}$$

With the usual expansion

$$\vec{n}_i = \vec{n}_i^{\,0} + \alpha_i \vec{a}_i + \beta_i \vec{b}_i - \tfrac{1}{2}(\alpha_i^2 + \beta_i^2)\vec{n}_i^{\,0} + \cdots \ .$$

for small deviations from equilibrium vectors $\vec{n}_i^0$, Eq. (4.10) leads in first order to the equations

$$\sum_j \hat{J}_{ij}(\alpha_j \vec{a}_i \cdot \vec{a}_j + \beta_j \vec{b}_i \cdot \vec{b}_j) - \alpha_i \hat{\lambda}_i = -\vec{a}_i \cdot \vec{h}_0 \ , \quad (4.11a)$$

$$\sum_j \hat{J}_{ij}(\alpha_j \vec{b}_i \cdot \vec{a}_j + \beta_j \vec{b}_i \cdot \vec{b}_j) - \beta_i \hat{\lambda}_i = -\vec{b}_i \cdot \vec{h}_0 \ . \quad (4.11b)$$

In vector form this becomes

$$\begin{bmatrix} A & B \\ B^T & C \end{bmatrix} \begin{pmatrix} \alpha_i \\ \beta_i \end{pmatrix} = - \begin{pmatrix} \vec{a}_i \cdot \vec{h}_0 \\ \vec{b}_i \cdot \vec{h}_0 \end{pmatrix} \ , \quad (4.12)$$

where

$$E = \begin{bmatrix} A & B \\ B^T & C \end{bmatrix}$$

is the matrix of the quadratic form for the energy for small displacements from equilibrium [see Eq. (2.5)]. Equation (4.12) can be solved by expanding

$$\begin{pmatrix} \alpha_i \\ \beta_i \end{pmatrix}$$

in terms of the eigenvectors of E having eigenvalues > 0. To ensure that the zero-energy eigenvectors are not admixed into

$$\begin{pmatrix} \alpha_i \\ \beta_i \end{pmatrix} \ ,$$

their projection onto the right-hand side of Eq. (4.12) is rendered zero by aligning $\vec{h}_0$ with the net moment $\vec{M} = \sum_i \vec{n}_i^0$ of the system. The susceptibility $\Delta|\vec{M}|/|\vec{h}_0|$ is then

$$\chi_{\rm at}(0) = N^{-1} \sum_\mu{}' \epsilon_\mu^{-1} \left(\sum_i (\xi_{\mu i} \vec{a}_i \cdot \vec{u}_0 + \eta_{\mu i} \vec{b}_i \cdot \vec{u}_0) \right)^2 \ , \quad (4.13)$$

where the μth eigenvector of E is

$$\begin{pmatrix} \xi_{\mu i} \\ \eta_{\mu i} \end{pmatrix} \ ,$$

with eigenvalues ϵ_μ, $\vec{u}_0 = \vec{h}_0/|\vec{h}_0|$, and $\sum'$ is taken over the $N-3$ eigenstates with $E_\mu > 0$. To convert $\chi_{\rm at}(0)$ to emu/mole, multiply by $N_0 c g^2 \mu_B^2 a^3 S/2\sqrt{2}A$. Apart from the changes in A [e.g., Eq. (4.8)], $\chi_{\rm at}(0)$ (emu/mole) is then independent of c as required by scaling.

Equation (4.13) has been employed to calculate $\chi_{\rm at}(0)$ for 10 systems of 96 spins at $c = 0.3$ at.%. The result is $\chi_{\rm at}(0) = 89.9 \pm 33\%$ ru. In addition to this, results from 10 EC's of 188 spins each with an applied field $h_0 = 0.0005$ gives $\chi_{\rm at}(0) = 110 \pm 33\%$ ru. What is striking here is the large error margins which occur with relatively large simulation samples, much greater than found in calculating the frequency spectra in Sec. IV C. Considerable insight into the reason for this can be gained through Eq. (4.13). Since the energies ϵ_μ vary over several orders of magnitude, Eq. (4.13) suggests that $\chi_{\rm at}(0)$ may be dominated by a small number of low-energy eigenstates. That this is the case is illustrated in Fig. 19, where we plot the susceptibility contribution of all eigenstates with energies less than ϵ_μ as a function of ϵ_μ. Results are shown for those 96-spin samples giving the largest and smallest susceptibilities. In both cases one finds large and widely varying contributions from a few states near the bottom. Thus a much greater number of simulation samples than one might have thought are required to produce statistically accurate results.

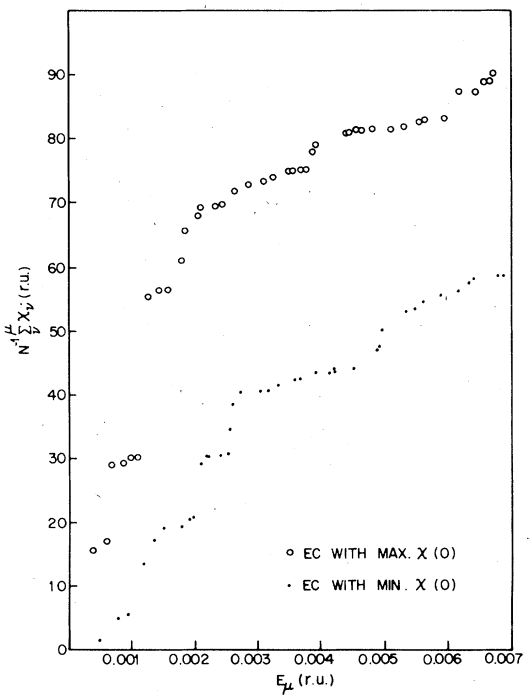

FIG. 19. Plot of accumulated energy eigenstate susceptibilities $\sum_{\nu \le \mu} \chi_\nu(0)$ vs ϵ_μ, where $\chi_\nu(0)$ is the summand in Eq. (4.13). Results from 96-spin EC's at $c = 0.3$ at.% with maximum (114) and minimum (82) $\chi(0)$'s are shown.

Equation (4.13) can also be recast in terms of individual spin contributions $\chi_i(0)$ to throw further light on the magnetization process. We plot $\chi_i(0)$ vs $\hat{\lambda}_i^{-1}$ in Fig. 20, since molecular-field models suggest that spins with small $\hat{\lambda}_i$'s should dominate $\chi_{\rm at}(0)$.[13] Not only is the correlation with $\hat{\lambda}_i^{-1}$ weak at best, there are many spins with $\chi_i(0) < 0$. Ferromagnetically coupled nearest-neighbor pairs are an interesting case in point. Although their λ_i's are large, such a pair can behave as a free spin if it is relatively isolated. The χ_i's for such pairs are seen to vary widely. Because of the strongly-interacting nature of the system

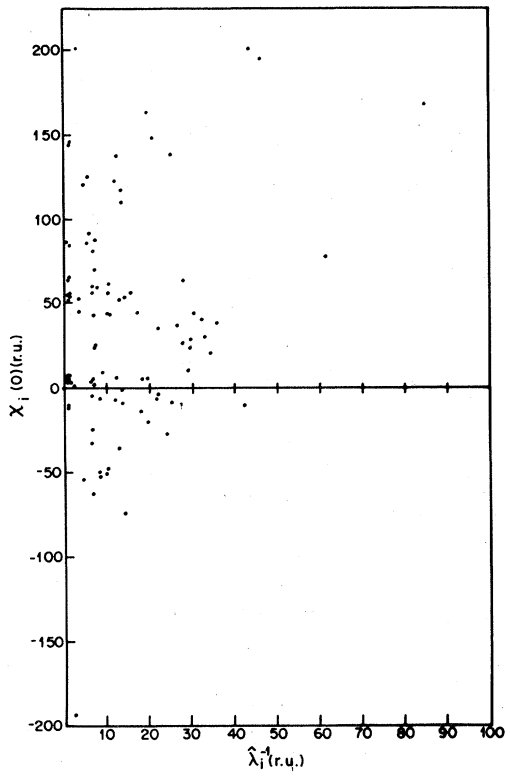

FIG. 20. Plot of individual spin susceptibility contributions $\chi_i(0)$ vs corresponding inverse molecular fields $\hat{\lambda}_i^{-1}$ for a system of 96 spins at $c = 0.9$ at.%.

there is no clear domination of $\chi_{at}(0)$ by a few large χ_i's.

We compare the calculated susceptibilities with the experimental data for *Cu*Mn and *Au*Fe in Table IV. The numbers we quote are from averages of both kinds of calculation described above. To evaluate the conversion factor given with Eq. (4.13) for *Cu*Mn we take $g = 1.65$ from $p_{\text{eff}} = 4.9$ (Ref. 37) and consider the variation of A with concentration discussed in Sec. IV C. The data in Table IV show the expected trend of increasing $\chi'(0)$ with c that follows from the decrease in A. Calculated values of $\chi'(0)$ are shown for $c = 0.9$ at.% and $c \to 0$, using the values of A and A_{eff} from the previous section. Although the error limits are large, the calculated results are in good accord with experiment.

Susceptibilities for *Au*Fe are smaller by a factor 2 or so than the *Cu*Mn values, but show a similar trend[13] with c. Diminished $\chi'(0)$ values are presumably a reflection of the smaller effective moment ($p_{\text{eff}} = 3.1$ from data in Ref. 13) for Fe impurities in Au. However, since $p_{\text{eff}} = g[S(S+1)]^{1/2}$, specific knowledge of g or S is required to discuss $\chi'(0)$ in detail. In the absence of such knowledge we may pursue a rough argument as follows. By comparing T_G and specific-heat data for *Au*Fe and *Cu*Mn one can deduce that S is smaller for the Fe moment than for Mn. This follows because even though there is no reliable theory of T_G, elementary theories of T_C and T_N for conventional ferro- and antiferromag-

TABLE IV. Comparison of extrapolated experimental values of $\chi_r(0)$ for *Cu*Mn and *Au*Fe with model calculations described in the text.

Authors	Alloy	$\chi_r(0)$
Cannella[a]	1.3 at.% Mn in Cu	1.4×10^{-3} (emu/mole)
Careaga *et al.*[b]	0.97 at.% Mn in Cu	2.0×10^{-3} (emu/mole)
Careaga *et al.*[b]	0.196 at.% Mn in Cu	1.0×10^{-3} (emu/mole)
Careaga *et al.*[b]	0.099 at.% Mn in Cu	1.0×10^{-3} (emu/mole)
Careaga *et al.*[b]	0.044 at.% Mn in Cu	1.0×10^{-3} (emu/mole)
Careaga *et al.*[b]	0.0186 at.% Mn in Cu	1.0×10^{-3} (emu/mole)
Present model	<0.1 at.% Mn in Cu	0.95×10^{-3} (emu/mole)
Present model	0.9 at.% Mn in Cu	1.70×10^{-3} (emu/mole)
Tholence and Tournier[c]	0.5 at.% Fe in Au	0.75×10^{-3} (emu/mole)
	0.2 at.% Fe in Au	0.53×10^{-3} (emu/mole)
Cannella and Mydosh[d]	1.0 at.% Fe in Au	0.41×10^{-3} (emu/mole)

[a]Reference 2.
[b]Reference 42.
[c]Reference 13.
[d]Reference 2.

nets[43] always give $T_{C,N} \propto S(S+1)$. It is reasonable, then, to take $T_G \propto V_0 S(S+1)$, where V_0 is the RKKY coefficient.[37] On the other hand, the temperature scale for $C_M(T)$ is proportional to $A = V_0 S$. Taking $c = 1$ at.% for example, one has from Sec. IV C $(V_0 S)_{\mathrm{Mn}}/(V_0 S)_{\mathrm{Fe}} \sim 0.85$, whereas $T_G(\mathrm{Mn})/T_G(\mathrm{Fe}) \sim 1.25$ (Refs. 13 and 39). This strongly suggests $S_{\mathrm{Fe}} < S_{\mathrm{Mn}}$. With the assignment $S_{\mathrm{Mn}} = \frac{5}{2}$, these numbers are consistent with $S_{\mathrm{Fe}} = \frac{3}{2}$. Adopting this, it follows from p_{eff} that $g = 1.60$ for Fe in Au. These parameters lead to an expected reduction of $\chi^r(0) \propto g^2 S/A_{\mathrm{eff}}$ for *Au*Fe by a factor 0.48 below the *Cu*Mn value, which is consistent with the data of Table IV. While the foregoing picture is somewhat speculative, it gives a consistent account of all the data available.

Returning to the discussion of the first paragraph, we conclude that $\chi^r(0)$ is accounted for the by the bulk-polarization contribution alone. However, let us estimate the "domain-rotation" contribution to $\chi^r(0)$ for $C_{0.99}Mn_{0.01}$ using Alloul's finding of a relatively uniform anisotropy field[26] $H_A \sim 1.3$ kG and an estimate of $n \sim 250$ for mean domain size.[13] Assuming the domains to be randomly oriented one finds

$$\chi^r(0)_{\mathrm{domain}} = \frac{2N_0 c g \mu_B S}{3\sqrt{n} H_A} \quad . \tag{4.14}$$

With the parameters quoted above this gives $\chi^r(0)$ (domains) $\sim 9 \times 10^{-3}$ emu/mole. Since this is larger than the experimental value one is forced to conclude with Alloul[26] that such domains are not present.

V. SUMMARY AND CONCLUSIONS

A simulation model has been developed to study the properties of spin-glasses at temperatures well below the ordering temperature T_G. Our procedure is patterned after the spin-wave treatment of multisublattice systems, treating deviations from a classical ground state in a quadratic Hamiltonian quantum approximation. The main investigation has been limited to (isotropic) RKKY exchange couplings with pilot studies of effects of small dipolar and local anisotropic terms and of an applied field.

With isotropic coupling the energies of distinct equilibrium configurations (EC's) were found to vary among themselves by less than 0.1%. In contrast, Ising equilibrium states were found to be considerably higher in energy and broadly distributed. In an extensive search, only seven unique EC's were found for a distribution of 172 spins, and all 7 have substantial mutual projection when inversion and rotation symmetry operations were optimized. Angular correlations of equilibrated spins have a very short range, with an average of only two neighbors within a suitably defined correlation volume. Angular correlations, as well as subsequent properties calculated, were found to obey the scaling laws appropriate to a system with inverse r^3 interactions.

The distribution of exchange fields $P(H)$ for disordered spins at $c = 0.3$ at.% was found to agree with a functional form derived in the limit $c \to 0$. Ordering was found to broaden $P(H)$ by $\sim 50\%$ and to reduce greatly the number of spins with very small fields. A single-particle specific-heat calculation based on $P(H)$ would clearly be unsuccessful.

A second-order expansion of the system Hamiltonian about a classical EC leads to a linearized set of equations of motion for creation and annihilation operators for local spin deviations. These equations are shown to be identical to the corresponding classical ones. The quantum equations are solved by the usual Bogoliubov transformation employed in multisublattice spin-wave theory with normalization imposed by the commutation relations. For a system of N spins the excitation frequencies, which occur in pairs $\pm\omega_\nu$, are the solutions of a non-Hermitian $2N \times 2N$ matrix. Expressions are given for the mean spin deviation at temperature T and the ground-state energy correction. In the Appendix there are shown to be three low-lying modes which are related to the full rotational symmetry of the system Hamiltonian. Such modes are believed to be unrelated to the thermodynamics of macroscopic spin-glasses and thus have been removed from calculated excitation spectra. Certain low-frequency macroscopic modes in spin-glasses have recently been calculated by Saslow[44]; we believe these to be unrelated to the modes considered in the Appendix.

Excitation spectra presented for series of $N = 96$ and 172 equilibrated spin distributions give similar results for the most part, with finite sample effects confined to the lowest frequencies. The spectra exhibit a low-frequency peak which evidently controls the low-temperature thermodynamics of the system; below the peak the mode density $N(\omega)$ diminishes rapidly, consistent with $N(0) = 0$ as required for the stability of the spin-wave-like solution to the Hamiltonian. The modes in the low-frequency peak are found to be moderately extended in space, although our sample size is too small to determine whether extended solutions with an associated wave vector exist as suggested by several authors.[6]

In studying the effect of various modifications to the Heisenberg RKKY interaction, we found that both dipolar and local (cubic) anisotropy have the effect of introducing a low-frequency gap in the spectrum when large enough. The classical dipolar interaction is too small, however, to have an appreciable effect. A similar gap is produced by an applied uniform field, the effect being rather modest for, e.g., 0.9 at.% Mn in Cu with $h_0 \sim 35$ kG. Exponential damping of the RKKY range function is found simply to scale the mode frequencies in the vicinity

of the peak to lower values, thus in effect to decrease the value of the RKKY coupling constant. The amount of scaling is comparable to the narrowing effect on field-component distributions reported earlier.[12]

Model specific-heat calculations are compared with recent data for *Cu*Mn (Refs. 32 and 33) and for *Au*Fe (Ref. 36). With the RKKY amplitude as the only adjustable parameter, we find good accord with data for 0.88 at.% Mn in Cu (Ref. 32) up to $T \sim \frac{1}{3} T_G$, as large a range as can be expected for this type of calculation. A small discrepancy near $T=0$ is attributed to finite sample distortion of the excitation spectrum. For 1 at.% Fe in Au, good agreement is found with experimental specific heat over a wider range of T, but with a much more serious discrepancy near $T=0$. There one finds a more nearly linear specific heat than the model can produce, a result very likely attributable to the Kondo effect in *Au*Fe. The concentration dependence of the *Cu*Mn specific-heat results is shown to be in accord with that of T_G and to be accountable in terms of self-damping of the RKKY interaction. Considering the effective c dependence of the RKKY coefficient A_{eff}, the value of A_{eff} derived for the 0.88 at.% Mn in the Cu case above is in reasonable agreement with the data of Smith.[37]

The classical model ground state yields an expression for the zero-temperature susceptibility in terms of the eigenfunctions and eigenvalues of the energy. Using $A_{\text{eff}}(c)$ from the specific-heat work, one finds values of $\chi(0)$ for *Cu*Mn in good accord with available data[2,42] including the trend with concentration. The diminished value of $\chi(0)$ for *Au*Fe as compared with *Cu*Mn is shown to be consistent with its lower T_G and larger specific heat in a picture where the Fe moment has a spin $S=\frac{3}{2}$. We have estimated the "domain rotation" contribution to $\chi(0)$ which would be present in the monodomain theory of spin-glass[13] in addition to the bulk-polarization result given by our model. Since the domain-rotation effect is large, we must conclude with Alloul[26] that such domains are absent in a zero-field cooled sample.

It should be emphasized that in our discussion of the excitations in this model system we have confined our attention entirely to the regime in which the equations of motion can be linearized. This will certainly exist below some temperature, but we have not considered how this limit might be determined. In order to do this it would be necessary to consider the interactions between the excitations and also the renormalization of their frequencies with increasing amplitude. These will presumably signal the first departures from the linear regime. Such problems are clearly very much more difficult here than in uniform systems, since we are linearizing the equation of motion of the individual spins, each of which has its own particular environment. Linearization may well be adequate for some spins and fail for others. A further effect, which presumably sets in at higher energies of excitation, is the migration of the system as a whole to the vicinity of another equilibrium configuration. To investigate this possibility it would be necessary to determine the path in configuration space between initial and final configurations which has the lowest maximum energy.

ACKNOWLEDGMENTS

The authors would like to thank S. Geschwind and J. Hauser for stimulating discussions, L. Kaufman for a matrix-solving routine and B. C. Chambers for help with the computations.

APPENDIX

In a numerical simulation of a random system with a limited number of spins, where one is trying to gather statistics from a number of samples, it is important to eliminate bias. This may arise in the present problem in connection with the counting of modes. All systems, small or large, with purely isotropic interactions will have some small number of zero-frequency modes associated with the rotational invariance. Clearly since these have negligible weight in a real system they should be excluded from the counting in a simulation. We shall examine these modes in some detail and conclude that 3 is the number to be dropped.

We approach this problem by relating it to the properties of the matrix, $(\mathcal{S})$, of the classical quadratic energy [Eq. (3.7)]. This can be written in the polarization representation as

$$(\mathcal{S}) = \begin{pmatrix} P & Q \\ Q^* & P^* \end{pmatrix} , \tag{A1}$$

where P and Q were defined by Eq. (3.13); we have $P^\dagger = P$ and $Q^T = Q$, so that $(\mathcal{S})$ is Hermitian. It has three zero eigenvalues corresponding to independent rotations of the system and the other eigenvalues are positive. In the Cartesian representation all eigenvectors are real so that in the polarization representation

$$(\mathcal{S}) = \begin{pmatrix} P & Q \\ Q^* & P^* \end{pmatrix} = \begin{pmatrix} w^+ \\ w^- \end{pmatrix} (\epsilon) (w^{-T} w^{+T}) , \tag{A2}$$

where w^+ and w^- are $N \times 2N$ matrices and $(w^+)^* = w^-$; (ϵ) is the diagonalized energy matrix. It will be convenient to add to the energy a term, $-\xi \sum_i \vec{n}_i^0 \cdot \vec{n}_i$, arising from a small "shattered" field, ξ, with $\xi > 0$. All eigenvalues in (ϵ) are then raised by ξ without changing the eigenvectors.

The frequency matrix [Eq. (3.12)] may be written

as

$$\begin{pmatrix} -1 & 0 \\ 0 & 1 \end{pmatrix}(\mathcal{E})$$

and is diagonalized by the transformation [see Eq. (3.19) with $f_i = z_i^+ g_i = z_i^-$]

$$\begin{pmatrix} (z^-)^* & z^+ \\ (z^+)^* & z^- \end{pmatrix}\begin{pmatrix} -\Omega & 0 \\ 0 & \Omega \end{pmatrix}\begin{pmatrix} (z^-)^* & z^+ \\ (z^+)^* & z^- \end{pmatrix}^{-1} = \begin{pmatrix} -1 & 0 \\ 0 & 1 \end{pmatrix}(\mathcal{E}) \ . \tag{A3}$$

$(\mathcal{E})$ may now be eliminated from Eqs. (A2) and (A3) to yield

$$(S)\begin{pmatrix} -\Omega & 0 \\ 0 & \Omega \end{pmatrix} = (w^{+T}w^- - w^{-T}w^+)(\epsilon)(S) \ , \tag{A4}$$

where

$$(S) = (w^{-T}w^{+T})\begin{pmatrix} (z^-)^* & z^+ \\ (z^+)^* & z^- \end{pmatrix} \ ,$$

(S) has the form $(s^* s)$, where s is a $2N \times N$ matrix. We may now consider only the equation

$$(s)(\Omega) = (w^{+T}w^- - w^{-T}w^+)(\epsilon)(s) = (K)(\epsilon)(s)$$

or

$$(K)(s)(\Omega) = (\epsilon)(s) \ , \tag{A5}$$

the last line following from $(K^2) = 1$. This, in turn, follows because

$$\begin{pmatrix} w^+ \\ w^- \end{pmatrix}$$

is unitary. We shall also need below the relations $K^T = -K$ and $K^* = -K$.

If $m,n = 1, 2, 3$ are associated with the rotational eigenvectors of $(\mathcal{E})$, $\mu, \mu' = 1, 2, \ldots, 2N-3$ with the remaining ones and ν with a frequency mode, we may write

$$\sum_n K_{mn} s_{n\nu} \Omega_\nu + \sum_\mu K_{m\mu} s_{\mu\nu} \Omega_\nu = \xi s_{m\nu} \ ,$$

$$\sum_n K_{\mu n} s_{n\nu} \Omega_\nu + \sum_{\mu'} K_{\mu\mu'} s_{\mu'\nu} \Omega_\nu = (\xi + \epsilon_\mu) s_{\mu\nu} \ . \tag{A6}$$

For a fixed ν we solve the second set of equations in the form

$$s_{\mu\nu} = \sum_{\mu'} (\xi + \epsilon - \Omega_\nu K')^{-1}_{\mu\mu'} \sum_n K_{\mu' n} s_{n\nu} \Omega_\nu \ ,$$

where K' is the $2N-3 \times 2N-3$ matrix with elements $K_{\mu\mu'}$. Substituting this result in the first set of Eqs. (A6) we obtain

$$\Omega_\nu \sum_n K_{mn} s_{n\nu} + \Omega_\nu^2 \sum_n \sum_{\mu\mu'} K_{m\mu} (\xi + \epsilon - \Omega_\nu K')^{-1}_{\mu\mu'} \times K_{\mu' n} s_{n\nu} = \xi s_{m\nu} \ , \tag{A7}$$

which is a formally exact reduction of the frequency problem to a set of three equations in $s_{1\nu}$, $s_{2\nu}$, and $s_{3\nu}$.

In a finite system there will be a finite interval between zero and the lowest positive eigenvalue of $(\mathcal{E})$ and, in this case, we may, for sufficiently small Ω_ν and ξ, replace $(\xi + \epsilon - \Omega_\nu K')^{-1}_{\mu\mu'}$ by $\epsilon_\mu^{-1} \delta_{\mu\mu'}$. We now have

$$\Omega_\nu \sum_n K_{mn} s_{n\nu} + \Omega_\nu^2 \sum_{\mu,n} K_{m\mu} \epsilon_\mu^{-1} K_{\mu n} s_{n\nu} = \xi s_{m\nu} \ . \tag{A8}$$

Making use of the fact that the matrix elements of K are pure imaginary and that K is antisymmetric one finds, on calculating the determinant associated with Eq. (A8), a cubic in Ω_ν^2. For small ξ, examination of this cubic indicates three possibilites, $\omega^2 = O(\xi^2)$, $\omega^2 = O(\xi)$, and $\omega^2 = O(1)$. Confining attention to $\Omega > 0$ there are thus two modes whose frequency goes to zero as $\xi \to 0$ and one which goes to a finite frequency. The latter appears in our experience to

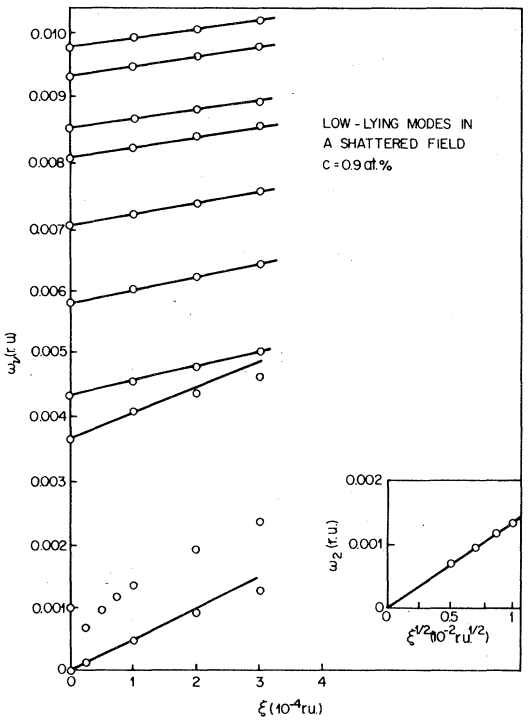

FIG. 21. Ten lowest mode frequencies for a sample of 96 spins at $c = 0.9$ at.% plotted as a function of the shattered field parameter ξ. The inset illustrates the $\xi^{1/2}$ behavior of the second mode.

have a frequency below that of the lowest positive energy mode so that its derivation as given here has some degree of self-consistency. From these results we conclude that three modes, two zero frequencies and the first positive frequency should be excluded from mode statistics. In Fig. 21 are shown the mode frequencies found by direct diagonalization as a function of ξ. The $\xi^{1/2}$ and ξ dependence of the lowest modes is clear; the next highest mode shows a dependence upon ξ which is distinct from all higher modes which move linearly with ξ.

It is possible to derive explicit expressions for the frequencies of these low-lying modes. The details are tedious and we shall not describe them; it is clear that they depend upon finding explicit expression for w^+ and w^-. The results are

$$\omega^2 = \xi^2 \frac{\det(R)}{\vec{M}^T(R)\vec{M}} \ ,$$
$$\omega^2 = \xi \frac{\vec{M}^T(R)\vec{M}}{\vec{M}^T(\chi)\vec{M}} \ , \qquad \text{(A9)}$$
$$\omega^2 = \frac{\vec{M}^T(\chi)\vec{M}}{\det(\chi)} \ ,$$

where $\vec{M} = \sum_i \vec{n}_i^0$ is the total moment, (R) is a 3×3 matrix whose elements are

$$R_{\alpha\beta} = N\delta_{\alpha\beta} - \sum_i n_i^{0\alpha} n_i^{0\beta} \ ,$$

where the $n_i^{0\alpha}$, $\alpha = x,y,z$, are the Cartesian components of $\vec{n}_i^0$ and (χ) is the dc susceptibility matrix mentioned in Sec. IV whose elements are

$$\chi_{\alpha\beta} = \sum_\mu m_\mu^\alpha \epsilon_\mu^{-1} m_\mu^\beta \ ,$$

where $\vec{m}_\mu$ is the total moment of the μth energy mode and $\alpha, \beta = x,y,z$.

It was mentioned in Ref. 25 that a slight complication appears in the quantum-mechanical diagonalization procedure. This is, in fact, connected with the zero-frequency modes and we discuss it briefly here. Suppose we form the vector operator $\vec{T}$, where [see Eq. (3.2) for notation]

$$\vec{T} = \sum_i (\vec{p}_i^- c_i^\dagger + \vec{p}_i^\dagger c_i) \ .$$

It is easily verified that $[\mathcal{H}_2, \vec{T}] = 0$, so that the components of $\vec{T}$ are constants of the motion. It is also true that

$$[T^x, T^y] = iM_z, \quad [T^y, T^z] = iM_x \ ,$$
$$[T^z, T^x] = iM_y \ ,$$

where $\vec{M} = \sum_i \vec{n}_i^0$ is the total moment of the system. If the z axis is chosen to lie along $\vec{M}$ then

$$[T^x, T^y] = i|M|, \quad [T^y, T^z] = 0, \quad [T^z, T^x] = 0 \ .$$

$T^+ = T^x + iT^y$ and $T^- = T^x - iT^y$ are Hermitian conjugates and may evidently, after normalization, be associated with the d and d^+ of one $\omega = \pm 0$ pair. This leaves one operator, T^z, which is a constant of the motion, which commutes with T^+ and T^-, but is unfortunately self-adjoint, so that it has no conjugate mate. This is an indication of the fact that the purely isotropic H_2 is not strictly diagonalizable in the sense of having a complete set of $2N$ linearly independent eigenfunctions. This difficulty, which has no adverse repercussions, occurs only for one $\omega = 0$ pair. It disappears in the presence of suitable perturbations.

If a dc magnetic field H_0 is applied in the direction of the total moment the system will reequilibrate. For the new equilibrium state we may define new operators T^+, T^-, and T^z obeying the same mutual commutation relations. The equations of motion of these operators are

$$\dot{T}^\pm = \mp H_0 T^\pm$$

and

$$\dot{T}^z = 0 \ .$$

This makes it clear that $T^\pm$ are associated with rotations in the plane normal to $\vec{M}$, and thus, with small precessional motions of $\vec{M}$ about the applied field; T^z, on the other hand, is connected with rotations of the whole system about the $\vec{M}$ axis. These considerations will apply to a macroscopic system in a field whose induced moment is of order N; in the absence of such a field the moment is of order $N^{1/2}$ and they are somewhat irrelevant.

[1]S. F. Edwards and P. W. Anderson, J. Phys. F 5, 965 (1975).

[2]V. Canella, in *Amorphous Magnetism*, edited by H. O. Hooper and A. M. de Graaf (Plenum, New York, 1973), p. 195; V. Canella and J. A. Mydosh, Phys. Rev. B 6, 4220 (1972).

[3]K. Binder, J. Phys. (Paris) 39, C6-1527 (1978), and references therein; see also W. Y. Ching and D. L. Huber, J. Phys. F 8, L63 (1978).

[4]K. Binder and K. Schröder, Phys. Rev. B 14, 2142 (1976); K. Binder, Physica (Utrecht) 86–88, B, 871 (1977); K. Binder, Z. Phys. B 26, 339 (1977).

[5]D. A. Smith, J. Phys. F 4, L266 (1974); F. Holtzberg, J. L. Tholence, and R. Tournier, in *Amorphous Magnetism II*, edited by R. A. Levy and R. Hasegawa (Plenum, New York, 1977), p. 155; K. Binder, Z. Phys. B 26, 339 (1977); C. M. Soukoulis and K. Levin, Phys. Rev. Lett. 39, 581 (1977); Phys. Rev. B 18, 1439 (1978); P. W. Anderson, J.

Appl. Phys. 49, 1599 (1978).
[6]At sufficiently low frequencies magnonlike excitation with definite wave vectors have been proposed to exist by B. I. Halperin and W. M. Saslow, Phys. Rev. B 16, 2154 (1977). Related papers are H. Takayama, J. Phys. F 8, 2417 (1978); and S. L. Ginzburg, Sov. Phys. JETP 48, 756 (1978).
[7]A similar study has been conducted by F. A. de Rozario, D. A. Smith, and C. H. J. Johnson, Physica (Utrecht) 86–88B, 861 (1977).
[8]L. R. Walker and R. E. Walstedt, Phys. Rev. Lett. 38, 514 (1977).
[9]W. Y. Ching, K. M. Leung, and D. L. Huber, Phys. Rev. Lett. 39, 729 (1977); D. L. Huber and W. Y. Ching, J. Appl. Phys. 49, 1633 (1978); D. L. Huber, W. Y. Ching, and M. Fibich, *ibid.* 50, 1739 (1979); W. Y. Ching, D. L. Huber, and K. M. Leung, (unpublished).
[10]M. A. Ruderman and C. Kittel, Phys. Rev. 96, 99 (1954); T. Kasuya, Prog. Theor. Phys. 16, 45 (1956); K. Yosida, Phys. Rev. 106, 893 (1957).
[11]J. Souletie and R. Tournier, J. Phys. (Paris) 32, C1-172 (1971).
[12]A clear-cut example of the breakdown of scaling with concentration may be found in our study of local-field distributions in systems with inverse r^3 potentials: Phys. Rev. B 9, 4857 (1974).
[13]J. L. Tholence and R. Tournier, J. Phys. (Paris) 35, C4-229 (1974).
[14]W. Marshall, Phys. Rev. 118, 1520 (1960).
[15]M. W. Klein and R. Brout, Phys. Rev. 132, 2412 (1963).
[16]N. Rivier and K. Adkins, in *Amorphous Magnetism,* edited by H. O. Hooper and A. M. de Graaf (Plenum, New York, 1973), p. 215; N. Rivier, Phys. Rev. Lett. 37, 232 (1976).
[17]W. Kinzel and K. H. Fischer, J. Phys. F 7, 2163 (1977).
[18]A. Freudenhammer, J. Magn. Magn. Mater. 7, 249 (1978); 9, 46 (1978).
[19]The symbols $\hat{J}_{ij}$ and $\hat{\lambda}_i$ are employed in the classical model of unit vector spins for the exchange and molecular-field constants, respectively. Their relation to their quantum-mechanical counterparts J_{ij} and λ_i, $\hat{J}_{ij}=SJ_{ij}$ and $\hat{\lambda}_i=S\lambda_i$, is derived in Sec. III, where S is the spin quantum number.
[20]Energies, exchange fields, and oscillation frequencies are all expressed in reduced energy units (ru). These are defined by setting $A=a^3/2\sqrt{2}$ in Eq. (2.9) so that the coefficient of $\cos(2k_Fr_{ij})$ is unity for nearest neighbors in the fcc lattice. The fcc lattice constant is a.
[21]C. Held and M. W. Klein, Phys. Rev. Lett. 35, 1783 (1975).
[22]R. G. Palmer and C. M. Pond, J. Phys. F 9, 1451 (1979).
[23]S. Kirkpatrick and C. M. Varma, Solid State Commun. 25, 821 (1978).
[24]Note that α_i and β_i are canonically conjugate variables; z_i^+ and z_i^- are not.
[25]See, for example, L. R. Walker, in *Magnetism,* edited by G. T. Rado and H. Suhl (Academic, New York, 1963), Vol. I, Chap. 8. A full discussion of the problem of diagonalizing quadratic Hammiltonians has been given recently by P. Broadbridge, Physica (Utrecht) 99 A, 494 (1979). A minor complication arising in the present problem is discussed in the Appendix.
[26]H. Alloul, Phys. Rev. Lett. 42, 603 (1979).
[27]P. Monod and J. J. Préjean, J. Phys. (Paris) 39, C6-910 (1978).
[28]R. A. Klemm, J. Phys. C 12, L735 (1979).
[29]The conversions of magnetic field $\vec{H}_0$ and classical dipolar coefficient $D=g^2\mu_B^2S$ to reduced units are $\vec{h}_0=(g\mu_Ba^3/2\sqrt{2}A)\vec{H}_0$ and $d=D/A$, respectively, where A is defined by Eq. (2.9).
[30]P. G. de Gennes, J. Phys. Radium 23, 630 (1962).
[31]M. Bloembergen and T. J. Rowland, Phys. Rev. 97, 1679 (1955).
[32]W. H. Fogle, J. C. Ho, and N. E. Phillips, J. Phys. (Paris) 39, C6-901 (1978).
[33]D. L. Martin, Phys. Rev. B 20, 368 (1979); 21, 1902 (1980).
[34]U. Larsen, Solid State Commun. 22, 311 (1977).
[35]L. E. Wenger and P. H. Keesom, Phys. Rev. B 13, 4053 (1976).
[36]L. E. Wenger and P. H. Keesom, Phys. Rev. B 11, 3497 (1975). We thank Professor Keesom for providing numerical tables of their $Au_{0.99}Fe_{0.01}$ specific-heat data.
[37]F. W. Smith, Phys. Rev. B 14, 241 (1976). In Smith's notation $A=V_0S$. We prefer to take $S=\frac{5}{2}$ and attribute the diminished saturation moment to $g<2$, leading to a slightly smaller value for A than is given by Smith's analysis.
[38]R. E. Walstedt, Bull. Am. Phys. Soc. 24, 304 (1979).
[39]V. Canella and J. A. Mydosh, in *Magnetism and Magnetic Materials—1973,* edited by C. D. Graham and J. J. Rhyne, AIP Conf. Proc. No. 18 (AIP, New York, 1973), p. 651; J. A. Mydosh, in *Magnetism and Magnetic Materials—1974,* edited by C. D. Graham, G. H. Lander, and J. J. Rhyne, AIP Conf. Proc. No. 24 (AIP, New York, 1974), p. 131.
[40]E. C. Hirschkoff, O. G. Symko, and J. C. Wheatley (referred to as HSW), J. Low Temp. Phys. 5, 155 (1971).
[41]The fact that the T_G/T_G (HSW) values do not extrapolate to unity at $c=0$ is presumably caused by a disparity in concentration calibration between Refs. 39 and 40.
[42]J. A. Careaga, B. Dreyfus, R. Tournier, and L. Weil, in *Proceedings of the Tenth International Conference on Low Temperature Physics, Moscow, U.S.S.R., 1966,* edited by A. S. Borovik-Romanov and V. A. Tulin (VINITI, Moscow, 1967), Vol. IV, p. 284.
[43]F. Keffer, in *Encyclopedia of Physics,* edited by S. Flügge (Springer-Verlag, New York, 1966), Vol. XVIII/2, p. 1.
[44]W. M. Saslow (unpublished).